Title: Flow directions and ages of subsurface water in a salt marsh system constrained by isotope tracing

Running title: Isotope tracing and water ages in a salt marsh

Authors: Emilio Grande[1,2 *], Ate Visser[3], Erik Oerter[3], Bhavna Arora[4], Erin C. Seybold[5], Corianne Tatariw[6], Anna Braswell[7, 8], Maya Montalvo[1, a], Margaret Zimmer[1]

[1] University of California Santa Cruz, Department of Earth and Planetary Sciences, Santa Cruz, CA, United States
[2] California State University East Bay, Department of Earth and Environmental Sciences, Hayward, CA, United States
[3] Lawrence Livermore National Laboratory, Nuclear and Chemical Sciences Division, Livermore, CA, United States
[4] Lawrence Berkeley National Laboratory, Energy Geosciences Division, Berkeley, CA, United States
[5] University of Kansas, Kansas Geological Survey, Lawrence, KS, United States
[6] University of Alabama, Department of Biological Sciences, Tuscaloosa, AL, United States
[7] University of Florida, School of Forest Resources and Conservation, Fisheries and Aquatic Sciences Program, Gainesville, FL, United States
[8] University Florida Sea Grant, Institute of Food and Agricultural Sciences, Gainesville, FL, United States
[a] Now at Simon Fraser University, Department of Geography, Burnaby, BC, Canada

Corresponding author: Emilio Grande
Department of Earth and Environmental Sciences, California State University East Bay, Hayward, CA 94542. email: emilio.grande@csueastbay.edu

Abstract:

Salt marshes are dynamic hydrologic systems where terrestrial groundwater, terrestrial surface water, and seawater mix due to bi-directional flows and pressure gradients. Due to the counteracting terrestrial and marine forcings that control these environments, we do not comprehensively understand water fluxes in these complex coastal systems. To understand the water sources, flow directions, and velocities in salt marsh porewater, we employed a combination of geochemical tracers and analytical models across a hillslope-to-salt marsh continuum in a salt marsh experiencing daily inundation of estuarine surface water (SW) from tides and mixing of fresh seasonal groundwater.

We used tritium (^{3}H) as a hydrologic tracer to assess porewater ages and stable water isotope (δ^2H and δ^{18}O) analyses to separate isotopically distinct estuarine and terrestrial groundwater across different depths and landscape positions in the study transect. We employed electrical conductivity to constrain the role of source mixing and evapotranspiration in salt marsh hydrology. Salinity and stable isotopes revealed that transpiration, rather than evaporation, increased subsurface water salinity to concentrations above estuarine SW during summer. Elevated salinity at depth indicated that salt marsh subsurface water is recharged during the dry growing season. Seasonal recharge patterns drive long-term deep subsurface water dynamics across the salt marsh, with ^{3}H ages of 3-7 years, and daily tidal cycles drive short-term shallow porewater dynamics with ^{3}H ages of 0 ± 3.6 years. Our conceptual understanding of the spatiotemporal changes in SW-subsurface water

interactions at the terrestrial-marine interface quantifies the hydrological constraints we are missing to improve our understanding of biogeochemical cycles within the salt marsh.

Key words
Salt marsh hydrology, coastal hydrology, porewater exchange, isotopic tracer, tritium age

1- Introduction

Salt marshes are dynamic hydrologic systems where terrestrial groundwater (GW), terrestrial surface water, and seawater mix. These systems play an essential role in global biogeochemical cycles, promoting carbon storage and nitrogen removal due to the saturated conditions resulting from frequent inundation (Robinson *et al.*, 2018). Further, salt marsh systems can act as buffers between the terrestrial-marine interface whereby terrestrially derived nutrients may be retained or processed, potentially lessening their effects on coastal environments (Kumar *et al.*, 2019). These processes are paramount, as excess nutrients released to coastal waters can enhance eutrophication and hypoxia (Peterson *et al.*, 2016), which may worsen with expected shifts in climatic patterns (Sinha *et al.*, 2017), and projected population growth in coastal areas (Neumann *et al.*, 2015). Thus, sustainable management of coastal waters is a critical environmental challenge due to these climatic and anthropogenic pressures on coastal zones (Ferguson and Gleeson, 2012). These challenges highlight the need for an improved understanding of terrestrial-marine interactions (Day *et al.*, 2008; Michael *et al.*, 2013), including water exchanges across the terrestrial-marine interface, particularly in salt marsh systems (Borja, 2005).

The hydrology of salt marshes is influenced by ecological and biogeochemical processes (Wilson *et al.*, 2015b), and it is complex due to the combined effect of diurnal, tidally driven water level oscillations (Grande *et al.*, 2022a), subsurface heterogeneity (Moffett *et al.*, 2012), and variable elevation gradients (e.g., microtopography; (Wang *et al.*, 2021b). For example, in lower marsh positions, along tidal channels, tidally driven water level fluctuations in tidal creeks induce hydraulic gradients that result in water circulation into and out of creek banks (Xin *et al.*, 2011). Further, secondary porosity due to animals that burrow in these low marsh areas (e.g., crab bioturbation; (Guimond *et al.*, 2020) impacts near-creek hydrology and can increase surface water-subsurface water exchanges (Xiao *et al.*, 2019). At higher elevations, middle and upper marsh positions are influenced by vertical hydraulic gradients caused by tidal inundation, evapotranspiration, precipitation, terrestrial runoff from contributing hillslopes, and terrestrial GW inputs (Xin *et al.*, 2013).

Several methods have been used to study surface water-GW interactions in coastal areas (Burnett *et al.*, 2006), which span various spatiotemporal scales (Guimond and Tamborski, 2021). Further, various methods tend to explain different driving forces. For local-to-regional spatial scales and over tidal cycles, seepage meters are an effective method for measuring surface water-GW exchanges directly (Rosenberry *et al.*, 2020). Hydraulic heads measured in groundwater wells at various depths and spatial extents are commonly used with Darcy's law to calculate surface water-GW exchanges (Wilson *et al.*, 2015a). The spatiotemporal resolution of groundwater wells is controlled by the spatial (and temporal) distribution of the wells. Numerical models have also been used across a broad spatiotemporal range (Reeves *et al.*, 2000). Naturally occurring tracers were helpful in studying surface water-GW exchanges in salt marshes (Xin *et al.*, 2022). For example, salinity mass balances provide quantifiable information across various spatiotemporal scales (Michael *et al.*, 2013). Isotope tracers, such as radon and radium isotopes, are widely used over short (Tamborski *et al.*, 2017; Coluccio *et al.*, 2021; Chen *et al.*, 2022) and long timescales (McKenzie *et al.*, 2021) to understand rates of subsurface-surface water exchanges. The stable isotopes of hydrogen and oxygen in water (δ^2H and δ^{18}O values) have also been used to study surface water-GW exchanges in coastal areas (Schmidt *et al.*, 2011; Wang *et al.*, 2021a).

Water stable isotopes (δ^2H and δ^{18}O values) are conservative tracers that help to explain mixing processes at the terrestrial-marine interface, aided by the significant isotopic contrast between terrestrial waters and seawater (Povinec *et al.*, 2008). Further, δ^2H and δ^{18}O values in water can trace local (Grande *et al.*, 2020), regional (Bowen *et al.*, 2022), and global hydrologic flowpaths

(Jasechko *et al.*, 2014). Thus, the relationship between δ^2H and δ^{18}O values is a practical tool for understanding water mixing at the terrestrial-marine interface (Debnath *et al.*, 2019). In addition, unlike salinity, which is affected by both evaporation and transpiration, δ^2H and δ^{18}O values are only altered by evaporation (Zhang *et al.*, 2010; Barbeta and Peñuelas, 2017). Therefore, δ^2H and δ^{18}O values have the potential to constrain evapotranspiration in salt marsh subsurface water and, in combination with salinity, understand the partitioning between evaporation and transpiration.

Tritium (^{3}H) in water is an additional isotope tracer that offers potential for studying surface water-GW exchanges at the terrestrial-marine interface. ^{3}H is the radioactive isotope of hydrogen (half-life = 12.3 years), and its radioactive decay results in a predicted activity concentration with time in GW from the moment water recharges the terrestrial aquifer, providing direct information on water residence time (Price *et al.*, 2003; Visser *et al.*, 2013). For example, ^{3}H has been used in coastal studies in combination with its decay product ^{3}He to calculate the apparent age distribution of the discharging GW offshore of south-eastern Sicily, Italy (Povinec *et al.*, 2006). The age of GW is essential for understanding subsurface flowpaths (Visser *et al.*, 2007), which can aid in understanding biogeochemical transformation processes in groundwater (Visser *et al.*, 2009). However, it is challenging to measure GW age distributions directly (Ekwurzel *et al.*, 1994). Another methodology to use ^{3}H to calculate subsurface water ages is to measure ^{3}H in local precipitation and calculate the decay time (Harms *et al.*, 2016). This technique is widely used in watershed hydrology to calculate stream water age distribution (Visser *et al.*, 2019; Grande *et al.*, 2020; Campbell *et al.*, 2021), and it offers potential for studying shallow subsurface water ages in salt marsh systems.

To advance our understanding of surface water-GW exchanges at the terrestrial-marine interface, we used a combination of isotopic and geochemical tracers (e.g., δ^2H, δ^{18}O, ^{3}H, and electrical conductivity) with analytical models that can help us understand the residence time distribution and the water sources across a salt marsh platform in the Elkhorn Slough National Estuarine Research Reserve in central California, USA. This Mediterranean system experiences semidiurnal tidal inundation of estuarine surface water in addition to fresh GW inputs, direct precipitation, and surface water inputs (e.g., agricultural drainage), which makes characterizing subsurface flowpaths challenging.

Our overarching objective was to develop an empirically informed conceptual model of water inputs/outputs and residence times in a salt marsh system by identifying what we hypothesize are the three dominant processes/drivers of water movement. First, we tested whether marked seasonal patterns in precipitation, common to the site's Mediterranean climate, affected terrestrial GW contributions to the salt marsh. Specifically, we studied the subsurface water flow directions and water sources across a hillslope-to-low marsh continuum. Secondly, to improve our understanding of subsurface flow velocities of salt marsh porewater, we calculated subsurface water ages and vertical recharge rates. Thirdly, we evaluated the relative role of evaporation and plant transpiration in increasing porewater salinity in the salt marsh.

2- Study area and measurements

This study was conducted at Elkhorn Slough (ES) in Monterey Bay, California (Figure 1A). The principal sources of surface freshwater to ES is Carneros Creek, an ephemeral stream that only flows during the wet winter months, and the Old Salinas River, a perennial stream, which discharges at the mouth of the slough (Caffrey and Broenkow, 2002). Other sources of freshwater are direct precipitation, and surface runoff via intermittent streams and channels that drain into the Slough (Figure S1).

Tides in the estuary are mixed semidiurnal with a mean range of 1.7 m, a spring tidal range of 2.5 m, and a neap tidal range of 0.9 m. The principal transport mechanism for water and nutrients in ES occurs via tidal exchange (Caffrey and Broenkow, 2002). Monterey Bay seawater reaches up to 6 km inland during high tides, and over 50% of the total water volume of the slough is flushed during each tidal cycle (Malzone, 1999).

The average precipitation in ES is 627 mm/year (based on 2001-2022 record), with ~ 90% of the precipitation falling between November and April as rain (Chapin *et al.*, 2004). Air temperature averages 11.1 ºC in the winter and 15.4 ºC in the summer (Caffrey, 2002). The Mediterranean climate of the study site results in marked wet/dry seasonal dynamics (Figure 2), which provide the conditions to resolve seasonal variations in climatic forcing that impact subsurface saturation and mixing of fresh and saline waters. In this area, the wet periods occur during the dormant winter season, while the dry periods occur during the summer growing season. Pickleweed, *Salicornia pacifica*, is the dominant marsh plant (Van Dyke and Wasson, 2005), and the dominant grazer and bioturbator is the lined shore crab, *Pachygrapsus crassipes* (Beheshti *et al.*, 2022).

2.1 Experimental Transect and hydrologic parameters measured

For this study, we focused on a 60 m experimental transect across a hillslope-to-salt-marsh continuum located in the upper northwest section of ES (Figure 1). The salt marsh section extends over the lower ~24 m of the transect with an elevation range of 0.24 m (all elevations relative to NAVD88). The salt marsh section of the transect is tidally influenced, with a local tidal range of -0.54 to 2.21 m. We delineated the salt marsh by elevation into upper (1.71 m), middle (1.65 m), and lower (1.59 m) positions based on differences in average tidal inundation duration: 5.4%, 7.2%, and 9.6%, respectively (Figure 1 B-C). Further, we demarcated an upland position ~6 m inland from the upper marsh within the terrestrial-marine transitional zone at an elevation of 2.78 m. We also designed a terrestrial position in the contributing hillslope, hereafter referred to as the hillslope position, ~30 m from the upland position, at an elevation of ~6 m (Figure 1 B-C).

To study the spatiotemporal variations of the salt marsh hydrology, we established a network of observation and sampling piezometers. At the three salt marsh positions, we installed a network of 70 cm below-the-ground-surface (bgs) observation piezometers where we measured water level at five-minute intervals with Solinst pressure transducer loggers (Levelogger 5,Ontario, Canada). The observation piezometers had a 15 cm screen at the bottom. At each marsh position, we installed shallow sampling piezometers at 10, 30, and 50 cm-bgs (Figure 1C). Further, at each transect position (hillslope to lower marsh), we established deeper piezometers of various depths (1-3 m-bgs) used for water sampling (Figure 1C, Table S1). Except for the hillslope piezometer, we measured water level at five-minute intervals with Solinst pressure transducer loggers in the deep piezometers (Table S1). We also used a Solinst pressure transducer to measure air pressure at the transect at five-minute intervals to barometrically correct the water pressure measurements to calculate the water level. Data gaps in the water level records of the deep piezometers caused by pumping during sampling varied between hours to weeks. However, because we did not use time series analysis in this study, we did not fill the data gaps (e.g., Figure 2B).

2.2 Ancillary data

To account for multiscale climate forcing (seasonal and sub-daily) effects on the salt marsh hydrology, we used hourly meteorological data from the Elkhorn Slough Meteorological Station, located ~4.5 km from the study site (36º48'55", -121º44'17"). The station is managed and maintained by the National Estuarine Research Reserve System (NERR, 2022). Our analyses used relative humidity, barometric pressure, precipitation, wind speed, total photosynthetically active radiation (PAR), and air temperature (Figure S2).

3- Methodology

3.1 Isotopic and electrical conductivity measurements

To improve our understanding of the surface water-GW exchanges at the terrestrial-marine interface, we conducted periodical subsurface, surface, and precipitation water sampling across the field site (Figure 2). Water samples were analyzed for three complementary tracers (electrical conductivity (EC), stable water isotopes, and tritium) that enabled us to understand different aspects of the salt marsh hydrology: the degree of mixing between terrestrial and marine sources, the effects of evaporation and transpiration, and water ages and flow velocities. EC/salinity is subject to mixing and concentration by evaporation and transpiration. Stable isotopes are subject to mixing and fractionation by evaporation only. With these two tracers, the degree of mixing and the partitioning between evaporation and transpiration could be established. Tritium is subject to mixing and radioactive decay. Combined with the mixing fractions derived from stable isotopes, tritium provides an estimate of water age and inversely flow velocity (Beyer *et al.*, 2014). The combined interpretation of these tracers also allowed us to evaluate the effect of temporal variability in the precipitation end-member signature.

To study the spatiotemporal distribution of different water sources, we collected and analyzed samples for stable water isotopes and EC from various depths (n = 86, Table S2). We collected precipitation water at the site using a precipitation funnel, the volume of collected water for each sample varied as a result of variability in precipitation intensity, amount and collection duration (Table 1). In addition, we collected a sample from the tidal creek in winter, during the rainy season (Figure 2), and and two irrigation water samples from the agricultural field above the study site (Figure 1A) which is pumped from local GW (~400 m bgs), hereafter referred to as deep GW. We analyzed ^{3}H in 22 piezometer samples collected from 11 positions and depths and calculated the mean ^{3}H in precipitation from 21 samples.

We analyzed the stable water isotope samples by cavity ring down spectroscopy in a Picarro L2130-i at the University of California Santa Cruz. We measured electric conductivity of the samples with a Orion Star™ A329 multiparameter meter (Thermo Fisher Scientific, Massachusetts, USA). We analyzed ^{3}H samples at Lawrence Livermore National Laboratory by helium-3 accumulation (Clarke *et al.*, 1976; Surano *et al.*, 1992).

3.2 Local meteoric water line and line conditioning excess

The local meteoric water line (LMWL) is the site-specific long-term covariation of δ^2H and δ^{18}O (Rozanski *et al.*, 1993). Thus, conceptually, the LMWL of an area is a simplified representation of the average δ^2H and δ^{18}O relationship in precipitation (Putman *et al.*, 2019). For this study, we calculated the LMWL using monthly δ^2H and δ^{18}O values from the Online Isotopes in Precipitation Calculator (Bowen and Revenaugh, 2003; Bowen, 2022) and calculated the unweighted, orthogonal-least-squares fit of the relationship between δ^2H and δ^{18}O at the site. This LMWL is a practical tool that provides a hydrologic framework for evaluating hydroclimatic processes such as evaporation.

We evaluated the spatiotemporal variations between δ^2H and δ^{18}O by calculating the deviations from the LMWL. We described these variations in terms of the line conditioning excess (lc-excess), where lc-excess = $\delta^2H - m * \delta^{18}O - b$ (Landwehr and Coplen, 2006), where m and b are the slope and the intercept of the LMWL, respectively. The lc-excess mathematically expresses the offset between the LMWL and the studied samples in dual-isotope space. Most precipitation water will lie close to the LMWL and have a nearly zero lc-excess. When water evaporates, it becomes enriched in heavy isotopes such that they deviate from LMWL, and the lc-excess value becomes progressively negative during evaporation. Therefore, lc-excess is a valuable indicator of evaporative fractionation. It is worth noticing that precipitation samples can naturally deviate from the LMWL and consequently have a nonzero lc-excess. These deviations are accredited to variations in moisture sources, air mass trajectories, and cloud processes (Dansgaard, 1964).

3.3 Mixing models, tritium ages and uncertainty estimations

We explained subsurface water flow directions by studying the different water sources in the salt marsh subsurface (e.g., terrestrial and marine/estuarine). For this, we used stable water isotopes as tracers. In the analysis, we identified two clear end members, Elkhorn Slough surface water, representing marine/estuarine surface water, and terrestrial water, represented by precipitation and deep GW sampled at the site. We calculated mixing ratios between terrestrial and marine (estuarine) water using end-member-mixing analysis, where

$$f_{ES} = \frac{C_S - C_P}{C_{ES} - C_P} \quad (1)$$

and

$$f_{ES} + f_P = 1 \quad (2)$$

Where f [%] is the calculated fraction of each end member (estuarine or precipitation/terrestrial, *ES* or *P*, respectively), and *C* is the tracer concentration (δ^{18}O value) in the end members *ES* and *P* and the sample (*s*). We quantify the uncertainty of the mixing using a Gaussian error propagation (Genereux, 1998) as:

$$W_{f_{ES}} = W_{f_P} = \sqrt{\left[\frac{f_P}{C_{ES} - C_P} W_{C_P}\right]^2 + \left[\frac{f_{ES}}{C_{ES} - C_P} W_{C_{ES}}\right]^2 + \left[\frac{-1}{C_{ES} - C_P} W_{C_S}\right]^2} \quad (3)$$

Where *W* is the error (analytical error/uncertainty of the tracer measurement).

To understand the flow velocities of subsurface water in the salt marsh, we measured ^{3}H activity in subsurface water across the experimental transect and compared that with ^{3}H activity in Elkhorn Slough surface water (SW) and precipitation. The ^{3}H activity in precipitation at Elkhorn Slough was based on a regional estimate of ^{3}H in precipitation for central coastal California (Harms *et al.*, 2016; Visser *et al.*, 2018) and ^{3}H in precipitation in the city of Oakland, 115 km north of the field site (Grande *et al.*, 2020). For samples that showed limited mixing with ES water (i.e. sourced from precipitation infiltration), we calculated the apparent tritium age (τ[year]) as:

$$\tau = \frac{ln(\frac{C_0}{C})}{\lambda} \quad (4)$$

Where λ [year^{-1}] is the ^{3}H decay constant (0.0563/year), C_0[pCi/L] is the initial ^{3}H activity concentration in precipitation, and C [pCi/L] is ^{3}H activity concentration in the sample. The apparent tritium age calculation is based on the assumptions that (1) the sample represents a single age (i.e. piston flow distribution model) and (2) that the input of tritium in precipitation has effectively been constant (i.e. was the same at the time of recharge as today). A detailed analysis (Supporting Information Text S1) of several age distribution models (e.g. exponential model, dispersion model) considering the historical peak of tritium in precipitation in the 1960s and 1970s showed that the apparent tritium age adequately reflects the mean residence time of most likely age models.

We calculated the error of the age σ_τ [yrs] resulting from the analytical uncertainty of the tritium measurement as:

$$\sigma_\tau = \lambda^{-1}\sqrt{\left(\frac{\sigma_C}{C}\right)^2 + \left(\frac{\sigma_{C_0}}{C_0}\right)^2} \quad (6)$$

Where σ_c [pCi/L] is the uncertainty of the ^{3}H activity concentration measured in the subsurface water sample, σ_{C_0} [pCi/L] is the uncertainty in initial ^{3}H concentration. For mixed samples with contributions of both terrestrial flow paths and ES surface water, the age uncertainty was propagated numerically, by adding random noise (n=1000, normal distribution, standard deviation equal to the measurement uncertainty) to the δ^{18}O and ^{3}H measurements. After performing the end-member mixing and age calculations on the ensemble, we report the mean and standard deviation of the ensemble.

For terrestrial sourced samples, we estimated recharge flow velocities (v_V [cm/yrs]) as:

$$v_V = \frac{\tau}{\Delta Z} \quad (7)$$

where ΔZ [cm] is the sample depth. We calculated recharge rates (q_V [cm/yrs]) as:

$$q_V = v_V \phi \quad (8)$$

Where ϕ is the porosity. We measured porosity and bulk density for each position from soil samples extracted during the installation of the piezometers (Grande *et al.*, 2022a).

Because of the study's various sampling depths and the differences in piezometer depths (less than 0.5 m and larger than 1.7 m), we grouped the sampling piezometers into shallow and deep samples (unless otherwise specified). We refer to samples from piezometers with depths ≤ 50 cm-bgs as shallow samples and samples from piezometers > 50 cm-bgs as deep samples.

3.4 Statistical analysis

We analyzed the normality of all of the data distributions using histograms and Shapiro-Wilk tests (Shapiro and Wilk, 1965) using the "shapiro.test" function in base R (R Core Team, 2021). We tested if the variations in porewater electrical conductivity (EC), ^{3}H, and stable water isotopes differed significantly among positions and depths using Levene's test (Schultz, 1985). We used a significance level (α) of 0.05 for statistical significance. We used the "leveneTest" function from the "car" package in R (Fox and Weisberg, 2019). We used the Kruskal-Wallis test (Breslow, 1970) to analyze if EC, ^{3}H, and stable water isotopes are identical for the wet and dry seasons and to evaluate differences in their porewater signature/activity across depths and positions. We used a level (α) of 0.05 for statistical significance. We used the "kruskal.test" function in base R (R Core Team, 2021) for this analysis. We further analyzed all the significant results with pairwise Mann-Whitney U test (Rosner and Grove, 1999) to correct the significance level for multiple comparisons.

4- Results

4.1 Salt marsh hydrology and regional climate

During the 2020 and 2021 water year study period, we observed precipitation totals of 395.1 mm and 280 mm, respectively (Figure 2A). These are both well below the twenty year mean annual precipitation for the area (627 mm). We also observed marked wet/dry seasonality in the fluctuations of the upland water level record (Figure 2B). Over the study period, we observed a difference of 1.34 m between the peak terrestrial GW level (2.75 m relative to NAVD88) in the wet periods and the lowest level in dry periods (1.39 m).

The terrestrial water level increases during precipitation events/periods (Figure 2B). Marsh subsurface water levels are subject to daily, biweekly and seasonal tidal cycle inundation dynamics (that vary due to the position of the moon/earth), resulting in multiple water level fluctuation frequencies (Grande *et al.*, 2022a). Subsurface water levels at the lower marsh position are consistently lower than at the upper and middle marsh positions during low tides, draining below the marsh land surface elevation in each tidal cycle (Figure 2 C-E). However, the subsurface water level in the upper and middle marshes did not drop below the marsh land surface elevation during the wet and dormant winter season. This indicates that the marsh does not drain substantially between daily tidal cycles during wet periods. As the system transitions into the dry seasons, we observed that the terrestrial GW levels decreased, and the salt marsh subsurface water levels in the middle and upper positions also dropped below the salt marsh surface between tidal inundation periods (Figure 2 B-E).

4.2 Electrical conductivity of salt marsh subsurface water

EC varied across sampling sites (Table 2), generally decreasing from Elkhorn Slough surface water (SW) and the salt marsh positions to the hillslope position (Figure 3A-D), although not all the positions had significantly different EC values (Table S3). Notably, the tidal creek EC was not significantly different from any other position. The median SW EC was 55.3 mS/cm and varied between 46.6 and 60.7 mS/cm during the dry and wet seasons, respectively (Figure 3A-D). However, wet/dry seasonality did not cause significant differences in the EC values of SW ($p = 0.8$). Upland, hillslope, and precipitation were all significantly lower than SW. EC did not differ significantly between SW and the three salt marsh positions ($p = 0.3$) because of significant seasonal variation in the variability of salt marsh EC. Additionally, upland, hillslope, and GW were all significantly lower than the EC in each of the salt marsh positions (Table S3).

During the dry season, porewater EC in all marsh positions was higher than EC in SW due to evapotranspiration (Figure 3A-D). We used this hyper-salinity (EC values elevated above SW) as a valuable geochemical tracer to understand deeper marsh water flow directions and sources. In contrast to the dry season, wet season EC in all three marsh positions varied from above SW EC to below SW EC due to mixing with either precipitation or terrestrial water sources (upland, GW). The variance of salt marsh porewater EC was more pronounced during the wet season than during the dry season. The varying degrees of mixing resulted in significant differences between the lower, the middle, and upper marsh positions during the wet season, but not during the dry season. The upper marsh position showed the largest range in EC values, indicating the largest degree of mixing with terrestrial sources. However, evaporation did not result in significant variations in hyper-salinity in salt marsh porewater EC during the dry season ($p = 0.6$, Figure 3 A-D) suggesting that a biological control (i.e., plant transpiration) places an upper limit to the process of salinity concentration.

The deep salt marsh samples had overall significantly higher EC than shallow salt marsh samples. This significant difference is caused by lower EC values in shallow piezometers as a result of mixing with precipitation or terrestrial water during the wet season (Figure 4 A). In contrast, there were no significant differences in salt marsh EC with depth for the dry season ($p = 0.2$, Figure 4D).

4.3 Stable water isotopes as tracers of subsurface water exchange in salt marsh systems

Stable water isotope values varied across the transect (Table 3). The stable water isotope analysis revealed two end members: SW (mean $\delta^{18}O = 0.22$ ‰), representing the marine end-member, and deep GW from the area (mean $\delta^{18}O = -5.93$ ‰), likely representing the long-term signature of local precipitation (Figure 5). Precipitation water collected at the site had a mean $\delta^{18}O$ and a standard deviation $\delta^{18}O$ of -4.99 ‰ and 1.38 ‰, respectively (Table 3). Terrestrial water samples (upland and hillslope) and wet season precipitation closely resemble the low $\delta^{18}O$ value of GW, while dry season precipitation shows a larger range in $\delta^{18}O$. The lower and middle marsh positions were significantly higher, and more similar to SW (i.e. not significantly different from SW), than the upper marsh and the other terrestrial samples (Figure 3 B-E, Table S4).

The effect of wet/dry seasonality in the three salt marsh positions resulted in significantly lower $\delta^{18}O$ values in the wet season than in the dry season (Figure 3 B-E) as a result of terrestrial inputs into the salt marsh. However, wet/dry seasonality did not affect the terrestrial positions (Figure 3 B-E).

During the wet season, the shallow samples were isotopically lighter (i.e. lower $\delta^{18}O$ values) than the deep samples as a result of terrestrial or precipitation inputs (Figure 4 B-E). However, in the dry season, shallow samples were isotopically heavier (i.e. higher $\delta^{18}O$ values) than the deep samples, possibly as a result of evaporative fractionation ($p = 0.02$, Figure 4 B-E). Moreover, for individual marsh positions, the differences in isotopic composition and depth were only significant for the lower and upper marsh positions in the wet season and the upper marsh in the dry season (Figure 4 B-E). The tidal creek sample collected after a precipitation event in the wet winter season (12/28/2021, Figure 2A) had an unusually light isotopic signature with $\delta^{18}O$ = -4 ‰, suggesting a large component of terrestrial water, and was similar to shallow samples collected in the lower marsh during the wet season (Figure 6).

4.3.1 Local meteoric water line and line conditioned excess

Based on interpolated δ^2H and $\delta^{18}O$ estimates of precipitation values in the area downloaded from the Online Isotopes in Precipitation Calculator database, the LMWL has a slope of 7.1 and an intercept of 1.6 (Figure 6). The different precipitation events we sampled at the site during the 2022 water year do not align with the LMWL or the volume-weighted mean of these local precipitation samples (Figure S3, Table 3). However, the deep GW samples fall on the LMWL, suggesting that this water is a good indicator of the long-term precipitation in the area (Figure 6).

Lc-excess varied among transect positions (Figure 3 C-D). Negative and near-zero lc-excess values in SW contrast with positive lc-excess in the upland, hillslope, deep GW, and precipitation samples (Table 3). However, we found that not all the relationships were significantly different (Table S5). Notably, the lc-excess differed significantly among the three salt marsh positions and the terrestrial positions (Figure S4). Further, we found that wet/dry seasonality did not result in significant differences in lc-excess in any position (p =0.6, Figure 3 C-F). lc-excess differed among shallow and deep samples in the salt marsh during the wet season, but not during the dry season ($p = 0.7$, Figure 4).

Typically, evaporative fractionation results in progressively lower lc-excess values as δ^2H and $\delta^{18}O$ shift along a line with a slope of 5. We find no clear indication of evaporative fractionation in our samples. While the lc-excess of marsh water varies between 7 ‰ and -2 ‰, the range of values can largely be explained by the mixing between precipitation (6-12 ‰), terrestrial sources (3-6 ‰), and SW (-1 - -3 ‰; Fig S4). In the dry season, several samples plot below the mixing line, with more negative lc-excess values than mixing could explain, suggesting limited effect of evaporative fractionation.

4.3.2 Estuarine surface water and terrestrial water mixing

The salt marsh positions had significantly higher fractions of SW than the upland and hillslope positions (Figure 7). However, not all salt marsh positions were significantly different from another (Table S6). Further, the upper marsh position differed significantly from the lower and middle marsh, and from the upland and hillslope positions (Table S6).

The effect of wet/dry seasonality was evident in the fractional mix of SW and terrestrial water. The fraction of SW water in the salt marsh was significantly larger in the dry season than in the wet season (Table 4). Notably, the median fraction of estuarine surface water varied between 0.64 and 0.83 in the upper marsh position for the wet and dry seasons, respectively. During the dry season, six samples had higher $\delta^{18}O$ than SW, and during the wet season, one sample had higher $\delta^{18}O$ than SW, resulting in fractional mixing ratios above 100% (Figure 7). However, we did not find significant differences in wet/dry seasonality for the upland and hillslope positions.

During the wet season, shallow samples had smaller fractions of SW than deep samples (Figure 8). These results contrast with the dry season, when shallow samples had higher fractions of

SW than the deep samples. This variation in shallow mixing ratios is caused by precipitation and terrestrial sources mixing in the shallow subsurface, while deep marsh water appears to have a more consistent origin.

4.4 Tritium as a salt marsh porewater age tracer

The activity of ^3H in precipitation was based on 21 samples collected between 2014 and 2022 (Table 5). ^3H activities for the available samples varied between 4.0 pCi/L and 14.5 pCi/L. Each sample represented between 0.2% and 7% of the total precipitation in the water year it was collected. Because we found no correlation with sample date ($R^2 < 0.01$), daily precipitation amount ($R^2 < 0.01$), mean daily temperature ($R^2 = 0.13$), or wind direction ($R^2 = 0.09$, Figure S5), we considered these values to be randomly sampled from the natural distribution of ^3H in precipitation and calculated the mean (8.6 pCi/L), standard deviation (3.3 pCi/L) and used the uncertainty around the mean (0.7 pCi/L) for uncertainty propagation.

^3H in subsurface water varied between 5.4 pCi/L and 1.9 pCi/L in the upland and lower marsh, respectively (Figure 9A). The deep GW sample contained less than 1 pCi/L ^3H (Figure 9B) suggesting it recharged entirely before the 1950s. Shallow samples had higher ^3H activity concentrations than the deep samples for these marsh positions (Figure 9A).

Along the transect, ^3H is subject to both mixing of different sources, and radioactive decay reflecting the time since infiltration. We used δ^{18} to evaluate mixing and reconstruct the initial ^3H concentration from which we calculated water age (Figure 9B). The upper, upland, and hillslope deep piezometer samples are mixtures between the terrestrial and ES water. The degree of mixing in the hillslope sample is negligible (f_ES = 0.03 +/- 0.03) and the apparent tritium age of 12.7 +/- 1.8 yrs. The degree of mixing in the upland sample is limited (f_ES = 0.20 +- 0.02) and the apparent tritium age in the shallower piezometer (250 cm) is younger (5.8 +/- 1.8 yrs) than in the deeper hillslope piezometer (430 cm). Due to the mixing in the Upper Marsh position (f_ES = 0.17 +- 0.03), the uncertainty associated with the apparent tritium age is larger (11.8+-5.6 yrs) but the age is within the range of the upland and hillslope piezometers, suggesting converging terrestrial flow paths mix with marsh subsurface water. ^3H activities of lower and middle positions cluster closely around the ES SW value, suggesting the activities are not affected by significant decay. Assuming the ES SW value as the initial concentration, the age in the middle marsh deep piezometer is 2.3+-4 yrs, providing an upper limit to the range of ages in the marsh.

The analysis of these ages results in varying values of recharge velocity and recharge rates along the transect. Recharge velocities of 34 and 43 cm/yr in the upland and hillslope positions (respectively) translate to a recharge rate of 13 cm/yr (considering differences in porosity). For the lower marsh positions, vertical flow velocities of more than 1 m/yr, based on the young ages in the deep piezometers, are consistent with the seasonal variability observed in the shallower piezometers. These differences in recharge velocities, and their corresponding recharge rates (Table 6), reflect different positions along flow paths with different origins and salinity, as demonstrated by the mixing ratios discussed previously.

5- Discussion

The results of this study provide important conceptual insights into surface water-subsurface water exchanges at the terrestrial-marine interface, especially for salt marsh systems. This study demonstrates that a combination of stable water isotopes, tritium, and electrical conductivity in subsurface water of a hillslope to salt marsh continuum is a valuable tool to understand the effect of wet/dry seasonality typical to Mediterranean climates in the subsurface flow direction and porewater exchange. Our general results on the hydrological processes of the salt marsh subsurface agree with previous studies based on numerical models informed by piezometers and seepage meters (Michael *et al.*, 2005), porewater salinity (Shen *et al.*, 2015), and radon isotopes (Smith *et al.*, 2008; Wang *et al.*, 2021c). However, our study provides additional insights on porewater flow velocities, subsurface saltmarsh water recharge, and discretizes evaporation and transpiration processes in the salt marsh subsurface.

5.1 Salt marsh subsurface water evapotranspiration signatures differ by season

Salinity concentration in salt marsh subsurface water at Elkhorn Slough is primarily controlled by plant transpiration as stable water isotopes revealed no major evaporative fractionation (Figure 6). Subsurface water salinity in the salt marsh, and consequently EC, can increase due to evaporation and plant transpiration, and decrease by dilution from lower salinity waters such as precipitation, SW, and fresh GW (Nuttle and Hemand, 1988; Miklesh and Meile, 2018). In Mediterranean climates, the growing season coincides with the dry season (Feng *et al.*, 2019), creating "ideal" conditions for high evapotranspiration that can result in elevated subsurface water EC during the dry summer season. Salinity at the surface varied between sub-SW in wet periods (due to precipitation and terrestrial, freshwater inputs, Figure 3A-D), similar to SW (during the transition between wet-dry seasonality), and elevated-SW (during the dry growing season, Figure 5). The absence of clearly evaporated samples, based on both lc-excess and stable water isotopes (Figure 3 C-F, Figure 6), suggests plant uptake of water as the dominant mechanism for excess EC in salt marsh subsurface water.

A special case of observation bias could also result in the lack of evidence for evaporative fractionation in the salt marsh subsurface while salinity is elevated above the SW source end-member: evaporated (fractionated) water is produced at the land surface, where it is frequently inundated and thus flushed out (Grande *et al.*, 2022a). During the study, we saw changes in the saturation stage in the salt marsh subsurface with different hydrologic dynamics during wet and dry periods (Figure 2 C-E). In the dry season, the salt marsh subsurface drains below the salt marsh elevation at intra-tidal scales, resulting in vertical hydraulic gradients that favors SW infiltration/recharge during spring tides. Plant uptake happens below the surface. Thus, inundation could not flush away high EC water resulting from transpiration. Periodic evaporation and recharge from lake beds during the Pleistocene at Gold Flat Playa (Nevada, USA) also resulted in elevated salinity without isotopic evidence of evaporative fractionation in the Pahute Mesa groundwater system (Kwicklis *et al.*, 2021).

5.2 Seasonality drives dry season recharge of hyper-salinity water to the salt marsh subsurface

Hyper-salinity is only found during the dry growing season in shallow salt marsh water, but is observed throughout the year in the deep salt marsh samples. As hyper-salinity is a result of evapotranspiration at the surface or at rooting depth, we believe the dry season shallow water is the source of the deep hyper-salinity water. This is evidence that recharge of the deep salt marsh system must occur during the dry growing season (Figure 10). This unusual timing of recharge is explained by the relatively lower deep groundwater levels during the dry season, which allow for downward vertical flow. Higher water tables during the wet season limit the downward vertical flow thus recharge cannot take place in winter. Salt marsh recharge has been studied in the context of the primary mechanisms by which the salt marsh subsurface is recharged. For example, freshwater can recharge the salt marsh subsurface vertically due to direct precipitation on the salt marsh (Hemond *et al.*, 1984), or from underlying aquifers (Nuttle and Harvey, 1995), laterally from upland terrestrial GW inflow (Wilson *et al.*, 2015b), or streams and drainage channels connected to the salt marsh (Zhao *et al.*, 2021). Further, salt marshes can also be recharged by saline water that occurs vertically during spring tides that flood the salt marsh or laterally through the drainage creek banks during rising tides (Harvey *et al.*, 1987). However, less is known about the temporal changes in salt marsh subsurface water recharge. Here, we showed that deep salt marsh samples are recharged during the dry growing season (Figure 10).

5.3 Subsurface flow direction across the hillslope to salt marsh continuum

Wet season precipitation increases terrestrial GW levels, driving observed salt marsh hydrologic patterns (Figure 2). In the wet season, precipitation recharges GW in the hillslope and upland positions, resulting in a hydraulic gradient from the upland towards the salt marsh. Stable water isotopes revealed a decrease in terrestrial source contribution from the upland to the lower salt marsh position (i.e., an increase in the fraction of SW coastward), confirming the water level measurements (Figure 7). The stable isotope data corroborated the trends in salinity that suggest that lower marsh positions are more often inundated. Our results align with previous estimations in other salt marsh systems using numerical models and salinity gradients that have suggested that upper marsh positions are more influenced by terrestrial waters than lower marsh positions (Wilson and Gardner, 2006; Wilson *et al.*, 2015b).

Identifying the terrestrial end-member is critical for understanding the interactions between terrestrial and marine waters, as it permits us to account for freshwater contributions to the coastal ocean. Most of the research at the terrestrial-marine interface focuses on identifying submarine GW discharge or porewater exchange fluxes. However, only recently some researchers have focused on identifying the fraction of terrestrial freshwater from marine water using, for example, airborne thermal infrared (Tamborski *et al.*, 2015), a combination of remote sensing and radon-222 (Cheng *et al.*, 2020), water balance of the discharging aquifer (Zhou *et al.*, 2019), salinity (Ibánhez *et al.*, 2021), and stable water isotopes (Rocha *et al.*, 2016; Wang *et al.*, 2021a). We observed that the isotopic signature of the hillslope and the upland positions was similar to the deep GW sample from the regional aquifer (Figure 7). It is worth noting that the deep GW sample might be fossil water and reflect paleoclimatic conditions, but its similarity with the water sampled from the hillslope and upland positions suggests this is not the case (Figure 6). Furthermore, the terrestrial end-member is not necessarily the same as the weighted precipitation average measured during the study due to land surface processes that can affect the isotopic composition of the sample during recharge (i.e., evaporation).

The lower and middle marsh positions have a dominant SW source, while the upper marsh position is always a mix of terrestrial and SW (Figure 7). Previous studies have successfully used salinity/EC to study marine intrusion/recharge in coastal areas (Michael *et al.*, 2003; Cardenas *et al.*, 2010; Santos *et al.*, 2021). However, EC was not a good tracer in this site because it is affected by evaporation and transpiration, resulting in a significant excess in subsurface water EC higher than the marine end-member for several samples (Figure 3). Stable water isotopes proved to be a more conservative tracer than EC and provided more robust estimations of the fractional mix of SW across the study transect (Figure 10).

Wet/dry seasonality drives the direction of subsurface water flow in the salt marsh system (Figure 7). These findings are also in line with previous work based on hydraulic gradients in coastal aquifers showing that a shift in the freshwater–saltwater interface, influenced by seasonal variations in terrestrial GW levels, can justify saline discharges that lag inland recharge cycles (Michael *et al.*, 2005). Our results show that SW is drawn into upper marsh positions as the terrestrial–marine water interface moves landward during the dry season and discharges back into estuarine waters as the interface moves coastward during wet periods (Figure 7A). We found a connection between this Mediterranean climate's marked wet/dry seasonality, controlling terrestrial hydrological processes, and the salt marsh subsurface water, influenced by estuarine water contributions. These hydrological fluxes are important drivers of biochemical processes and chemical loadings in coastal waters that have shown shifts in salt marsh biogeochemical behavior as a function of wet/dry seasonality (Grande *et al.*, 2022b). The wet/dry seasonality results in significant shifts of the terrestrial-marine water interface across depths. However, the seasonality is limited to the shallow marsh, with more variable ranges of estuarine water fraction during wet periods. In contrast, the deep salt marsh sample did not experience significant shifts in the water sources across wet and dry periods.

On shorter time scales, hydrological fluxes are driven by precipitation, as precipitation water exchanges with shallow salt marsh subsurface water, leading to distinct isotopic signatures (similar to terrestrial water sources) in the tidal creek and shallow subsurface water samples collected during and after episodic precipitation events (Figure 6). Notably, many of these samples were collected during spring tides, thus our findings show that terrestrial water inputs to the salt marsh are not significantly diluted by frequent tidal inundation. During precipitation events, terrestrial water can be delivered to the salt marsh as overland flow through the intermittent streams and drainage network at the study transect (Figure S1), by infiltration of direct precipitation on the salt marsh, or by subsurface flow as the hillslope and upland positions become saturated and contribute freshwater to the shallow salt marsh subsurface. Recent work conducted at this site using high-frequency measurements of subsurface water nitrate (Grande *et al.*, 2022b) and wavelet and information theory on continuous redox potential (Grande *et al.*, 2022a) have proposed that precipitation water disturbed the subsurface water chemistry at shallow depths (down to 50 cm-bgs) over short periods from the onset of precipitation. Our results using stable water isotopes confirm these previous findings.

5.4 Tritium ages constrain subsurface flow velocities and recharge rates

While the shallow (10-50 cm) depths of the salt marsh are flushed regularly by tidal inundation (Grande *et al.*, 2022a), tritium ages show water moves through the deeper (~3 m) salt marsh on a time scale of 0-6 years. These ages constrain the water recharge component of subsurface flow velocities to 34-43 cm per year (Table 6). The substantial uncertainty (1.7-5.6 yrs) of the age estimates, and consequently the velocities, stems from the reconstruction of the initial ^{3}H activity concentrations of mixed samples (based on $\delta^{18}O$) as well as input variability. These initial tritium-based velocity estimates provide valuable constraints to numerical models aimed at understanding the complex three-dimensional transient subsurface flow field.

Shallow salt marsh porewater has been proposed to have short residence times throughout the literature. Researchers have found that shallow subsurface waters in marsh systems are affected by near-surface and lateral flow paths, resulting from tidal inundations and tidal pumping, with short residence times (Tamborski *et al.*, 2021). Other researchers have used radon mass balances to study lateral fluxes of carbon and methane from a low salt marsh position to a tidal creek, finding high fluxes from shallow samples that suggest short residence times (Chen *et al.*, 2022). These findings have been mostly described in lower marsh positions, where hydraulic conductivity is usually higher (Xiao *et al.*, 2019). However, using a tracer specific for subsurface water dating, we show that short residence times are expected in shallow subsurface waters across higher marsh positions as well. Tritium ages and recharge flow velocities, in combination with radiocarbon analyses, are powerful constraints for the interpretation and quantification of carbon turnover times, such as salt marshes or peatland ecosystems (Wilson *et al.*, 2021).

Subsurface water ages in the deep samples varied along the transect. In the lower salt marsh, subsurface waters are younger and recharge flow velocities are higher, indicating a short water residence time in this position and a more frequent surface water-subsurface water exchange (Table 6). This observation aligns with the conceptual understanding of lower marsh positions, which are more affected by secondary porosity, such as animal burrows, and thus have higher hydraulic conductivity that favors water circulation (Guimond and Tamborski, 2021). The deep middle and upper marsh positions presented water ages from a few years to a decade (Table 6). The isotopic composition of the deep samples did not vary significantly during the study period (Figure 4B-E), confirming that these positions have a longer residence time and that this water is not affected by episodic events, such as king tides or precipitation events.

5.5 Implications for carbon storage and water quality

The short residence time of shallow subsurface water in the salt marsh has important implications for our conceptual understanding of carbon storage in salt marsh systems. Given their high rates of primary productivity and slow decomposition in anoxic soils, salt marshes can store carbon for extended periods (Kathilankal *et al.*, 2008). However, soil oxidation, due to the circulation of oxygen-rich surface water recharging the shallow salt marsh subsurface, with a short residence time, has the potential to increase carbon oxidation and release back into the atmosphere (Lee, 2008). Further, surface water-subsurface water exchanges with short residence times have been observed to increase the lateral flux of inorganic carbon from salt marshes to the coastal ocean (Chen *et al.*, 2022).

The bimodal time-scales of subsurface water cycles in the salt marsh system can influence our understanding of nutrient budgets, such as nitrate, and the overall water quality of coastal zones. In systems such as Elkhorn Slough, where high nitrate concentrations are a water quality concern that has resulted in eutrophication events (Hicks *et al.*, 2019), understanding the water flow velocity and residence time of subsurface salt marsh water is valuable in evaluating total nutrient loads or removal potential. Our analysis can improve the understanding of nitrate retention in the salt marsh system, which had not been considered in this area (Broenkow and Breaker, 2019; Van Dop *et al.*, 2019). On the one hand, a long residence time of deep subsurface water, recharged in the summer, can potentially retain nitrate by dissimilatory nitrate reduction to ammonium due to the accumulation of recalcitrant carbon and sulfides in deep marsh sediments (Koop-Jakobsen and Giblin, 2009). In contrast, short residence time and fast exchange of shallow subsurface water with SW are influenced by oxygen and nutrient-rich surface water to labile carbon-rich shallow sediments that can result in nitrogen removal (denitrification) dominating over retention (Almaraz *et al.*, 2020).

6- Conclusion

The results of this study provide an empirically-informed conceptual model into salt marsh water recharge and subsurface flow paths. We found that subsurface water cycling has two dominant frequencies, seasonal patterns of terrestrial inputs that interact with daily tidal cycles driving short-term porewater dynamics in the shallow salt marsh. In summer, the water sources in the shallow marsh are controlled by tidal inundation and pore water uptake by vegetation. During the wet winter season, precipitation and terrestrial sources mix with daily inputs of SW. This results in fast water cycling in the shallow and lower marsh positions, but slower downward flow paths to deeper parts of the subsurface in the upper marsh, upland and hillslope positions.

Plant transpiration is the principal driver of increased salinity, because no evidence of evaporative fractionation is present. Our conceptual model suggests that deeper salt mash subsurface water is preferentially recharged with this super-saline water that was formed during summer by plant transpiration, while local winter precipitation recharges the terrestrial positions. Understanding the subsurface hydrology and the spatiotemporal variability of interacting hydro-geochemical processes in these dynamic hydrologic systems where terrestrial groundwater, terrestrial surface water, and seawater mix is essential for understanding how salt marshes might respond to disturbance or climate change.

Acknowledgements: The authors sincerely thank John Haskins from the Elkhorn Slough National Estuarine Research Reserve for field support. We also thank Peter Willits, Michael Wilshire, Jasper Romero and Adam Haynes for field assistance. EG was partially funded by a Cota-Robles Fellowship through the University of California Santa Cruz and by a NOAA Margaret A. Davidson fellowship (NA20NOS4200122). We acknowledge support from the NITRATES Project, funded by the U.S. Department of Energy, Office of Science, Office of Biological and Environmental Research, Award Number DE-SC0021044. We acknowledge support from a California SeaGrant under California Natural Resources Agency Award Number C0303100.

Data availability: Upon acceptance for publication, the data supporting this manuscript will be uploaded to an open source repository (DOE-managed ESS DIVE). The codes used in the manuscript will be uploaded to the corresponding author's GitHub page.

7- References

Almaraz M, Wong MY, Yang WH. 2020. Looking back to look ahead: a vision for soil denitrification research. *Ecology* **101** (1): e02917 DOI: https://doi.org/10.1002/ecy.2917

Barbeta A, Peñuelas J. 2017. Relative contribution of groundwater to plant transpiration estimated with stable isotopes. *Scientific Reports* **7** (1): 10580 DOI: 10.1038/s41598-017-09643-x

Beheshti K, Endris C, Goodwin P, Pavlak A, Wasson K. 2022. Burrowing crabs and physical factors hasten marsh recovery at panne edges. *PLOS ONE* **17** (1): e0249330 DOI: 10.1371/journal.pone.0249330

Beyer M, Morgenstern U, Jackson B. 2014. Review of techniques for dating young groundwater (<100 years) in New Zealand. *Journal of Hydrology (New Zealand)* **53** (2): 93–111

Borja Á. 2005. The European water framework directive: A challenge for nearshore, coastal and continental shelf research. *Continental Shelf Research* **25** (14): 1768–1783 DOI: 10.1016/j.csr.2005.05.004

Bowen G. 2022. The Online Isotopes in Precipitation Calculator, OIPC3.1. *http://www.waterisotopes.org.*

Bowen GJ, Revenaugh J. 2003. Interpolating the isotopic composition of modern meteoric precipitation. *Water Resources Research* **39** (10): 13 DOI: doi:10.1029/2003WR002086

Bowen GJ, Guo JS, Allen ST. 2022. A 3-D groundwater isoscape of the contiguous USA for forensic and water resource science. *PLOS ONE* **17** (1): e0261651 DOI: 10.1371/journal.pone.0261651

Breslow N. 1970. A Generalized Kruskal-Wallis Test for Comparing K Samples Subject to Unequal Patterns of Censorship. *Biometrika* **57** (3): 579–594 DOI: 10.2307/2334776

Broenkow WW, Breaker LC. 2019. A 30-Year History of the Tides and Currents in Elkhorn Slough, California. *Estuaries and Coastal Zones - Dynamics and Response to Environmental Changes* DOI: 10.5772/intechopen.88671

Burnett WC, Aggarwal PK, Aureli A, Bokuniewicz H, Cable JE, Charette MA, Kontar E, Krupa S, Kulkarni KM, Loveless A, et al. 2006. Quantifying submarine groundwater discharge in the coastal zone via multiple methods. *The Science of the Total Environment* **367** (2–3): 498–543 DOI: 10.1016/j.scitotenv.2006.05.009

Caffrey JM. 2002. Chapter 3: Climate. In *Changes in a California Estuary: An Ecosystem Profile of Elkhorn Slough*, Caffrey JM, , Brown M, , Tyler B, , Silberstain M (eds).Elkhorn Slough Fundation: Moss Landing, California; 25–28. Available at: http://library.elkhornslough.org/attachments/Caffrey_2002_Changes_In_A_California.pdf [Accessed 20 March 2022]

Caffrey JM, Broenkow W. 2002. Chapter 4: Hydrography. In *Changes in a California Estuary: An Ecosystem Profile of Elkhorn Slough*, Caffrey JM, , Brown M, , Tyler B, , Silberstain M (eds).Elkhorn Slough Fundation: Moss Landing, California; 29–42. Available at: http://library.elkhornslough.org/attachments/Caffrey_2002_Changes_In_A_California.pdf [Accessed 20 March 2022]

Campbell ÉMS, Lagasca PA, Stanic S, Zhang Y, Ryan MC. 2021. Insight into watershed hydrodynamics using silica, sulfate, and tritium: Source aquifers and water age in a mountain river. *Applied Geochemistry* **132**: 105070 DOI: 10.1016/j.apgeochem.2021.105070

Cardenas MB, Zamora PB, Siringan FP, Lapus MR, Rodolfo RS, Jacinto GS, San Diego-McGlone ML, Villanoy CL, Cabrera O, Senal MI. 2010. Linking regional sources and pathways for submarine groundwater discharge at a reef by electrical resistivity tomography, 222Rn, and salinity measurements. *Geophysical Research Letters* **37** (16) DOI: 10.1029/2010GL044066

Chapin TP, Caffrey JM, Jannasch HW, Coletti LJ, Haskins JC, Johnson KS. 2004. Nitrate sources and sinks in Elkhorn Slough, California: Results from long-term continuous in situ nitrate analyzers. *Estuaries* **27** (5): 882–894 DOI: 10.1007/BF02912049

Chen X, Santos IR, Hu D, Zhan L, Zhang Y, Zhao Z, Hu S, Li L. 2022. Pore-water exchange flushes blue carbon from intertidal saltmarsh sediments into the sea. *Limnology and Oceanography Letters*: lol2.10236 DOI: 10.1002/lol2.10236

Cheng KH, Luo X, Jiao JJ. 2020. Two-decade variations of fresh submarine groundwater discharge to Tolo Harbour and their ecological significance by coupled remote sensing and radon-222 model. *Water Research* **178**: 115866 DOI: 10.1016/j.watres.2020.115866

Clarke WB, Jenkins WJ, Top Z. 1976. Determination of tritium by mass spectrometric measurement of 3He. *The International Journal of Applied Radiation and Isotopes* **27** (9): 515–522 DOI: 10.1016/0020-708X(76)90082-X

Coluccio KM, Santos IR, Jeffrey LC, Morgan LK. 2021. Groundwater discharge rates and uncertainties in a coastal lagoon using a radon mass balance. *Journal of Hydrology* **598**: 126436 DOI: 10.1016/j.jhydrol.2021.126436

Dansgaard W. 1964. Stable isotopes in precipitation. *Tellus* **16** (4): 436–468 DOI: 10.1111/j.2153-3490.1964.tb00181.x

Day JW, Christian RR, Boesch DM, Yáñez-Arancibia A, Morris J, Twilley RR, Naylor L, Schaffner L, Stevenson C. 2008. Consequences of Climate Change on the Ecogeomorphology of Coastal Wetlands. *Estuaries and Coasts* **31** (3): 477–491 DOI: 10.1007/s12237-008-9047-6

Debnath P, Das K, Mukherjee A, Ghosh NC, Rao S, Kumar S, Krishan G, Joshi G. 2019. Seasonal-to-diurnal scale isotopic signatures of tidally-influenced submarine groundwater discharge to the Bay of Bengal: Control of hydrological cycle on tropical oceans. *Journal of Hydrology* **571**: 697–710 DOI: 10.1016/j.jhydrol.2019.01.077

Ekwurzel B, Schlosser P, Smethie WM, Plummer LN, Busenberg E, Michel RL, Weppernig R, Stute M. 1994. Dating of shallow groundwater: Comparison of the transient tracers ^{3}H/^{3}He, chlorofluorocarbons, and ^{85}Kr. *Water Resources Research* **30** (6): 1693–1708 DOI: 10.1029/94WR00156

Feng X, Thompson SE, Woods R, Porporato A. 2019. Quantifying Asynchronicity of Precipitation and Potential Evapotranspiration in Mediterranean Climates. *Geophysical Research Letters* **46** (24): 14692–14701 DOI: 10.1029/2019GL085653

Ferguson G, Gleeson T. 2012. Vulnerability of coastal aquifers to groundwater use and climate change. *Nature Climate Change* **2** (5): 342–345 DOI: 10.1038/nclimate1413

Fox J, Weisberg S. 2019. *An R Companion to Applied Regression*. Sage: Thousand Oaks, CA\. Available at: https://socialsciences.mcmaster.ca/jfox/Books/Companion/

Genereux D. 1998. Quantifying uncertainty in tracer-based hydrograph separations. *Water Resources Research* **34** (4): 915–919 DOI: 10.1029/98WR00010

Grande E, Arora B, Visser A, Montalvo M, Braswell A, Seybold E, Tatariw C, Beheshti K, Zimmer M. 2022a. Tidal frequencies and quasiperiodic subsurface water level variations dominate redox dynamics in a salt marsh system. *Hydrological Processes* **36** (5): 1–16 DOI: 10.1002/hyp.14587

Grande E, Seybold EC, Tatariw C, Visser A, Braswell AE, Arora B, Birgand F, Haskins J, Zimmer MA. 2022b. Seasonal and Tidal Variations in Hydrologic Inputs Drive Salt Marsh Porewater Nitrate Dynamics DOI: 10.1002/essoar.10511951.1

Grande E, Visser A, Moran JE. 2020. Catchment storage and residence time in a periodically irrigated watershed. *Hydrological Processes* **34** (14): 1–17 DOI: 10.1002/hyp.13798

Guimond J, Tamborski J. 2021. Salt Marsh Hydrogeology: A Review. *Water* **13** (4): 543 DOI: 10.3390/w13040543

Guimond JA, Seyfferth AL, Moffett KB, Michael HA. 2020. A physical-biogeochemical mechanism for negative feedback between marsh crabs and carbon storage. *Environmental Research Letters* **15** (3): 034024 DOI: 10.1088/1748-9326/ab60e2

Harms PA, Visser A, Moran JE, Esser BK. 2016. Distribution of tritium in precipitation and surface water in California. *Journal of Hydrology* **534**: 63–72 DOI: 10.1016/j.jhydrol.2015.12.046

Harvey JW, Germann PF, Odum WE. 1987. Geomorphological control of subsurface hydrology in the creekbank zone of tidal marshes. *Estuarine, Coastal and Shelf Science* **25** (6): 677–691 DOI: 10.1016/0272-7714(87)90015-1

Hemond HF, Nuttle WK, Burke RW, Stolzenbach KD. 1984. Surface Infiltration in Salt Marshes: Theory, Measurement, and Biogeochemical Implications. *Water Resources Research* **20** (5): 591–600 DOI: 10.1029/WR020i005p00591

Hicks K, Jeppesen R, Haskins J, Wasson K. 2019. Long-term trends and spatial patterns of water quality in estuarine wetlands of central California. Elkhorn Slough Technical Report Series. Scientific Report 2019:1. Elkohrn Slough NERR, Moss Landing, California. Available at: http://library.elkhornslough.org/research/bibliography/Hicks_2019_Long-term_trends_and_spatial.pdf [Accessed 11 April 2022]

Ibánhez JSP, Álvarez-Salgado XA, Nieto-Cid M, Rocha C. 2021. Fresh and saline submarine groundwater discharge in a large coastal inlet affected by seasonal upwelling. *Limnology and Oceanography* **66** (6): 2141–2158 DOI: 10.1002/lno.11733

Jasechko S, Birks SJ, Gleeson T, Wada Y, Fawcett PJ, Sharp ZD, McDonnell JJ, Welker JM. 2014. The pronounced seasonality of global groundwater recharge. *Water Resources Research* **50** (11): 8845–8867 DOI: 10.1002/2014WR015809

Kathilankal JC, Mozdzer TJ, Fuentes JD, D'Odorico P, McGlathery KJ, Zieman JC. 2008. Tidal influences on carbon assimilation by a salt marsh. *Environmental Research Letters* **3** (4): 044010 DOI: 10.1088/1748-9326/3/4/044010

Koop-Jakobsen K, Giblin AE. 2009. Anammox in Tidal Marsh Sediments: The Role of Salinity, Nitrogen Loading, and Marsh Vegetation. *Estuaries and Coasts* **32** (2): 238–245 DOI: 10.1007/s12237-008-9131-y

Kumar P, Dasgupta R, Johnson BA, Saraswat C, Basu M, Kefi M, Mishra BK. 2019. Effect of Land Use Changes on Water Quality in an Ephemeral Coastal Plain: Khambhat City, Gujarat, India. *Water* **11** (4): 724 DOI: 10.3390/w11040724

Kwicklis E, Farnham I, Hershey RL, Visser A, Hoaglund J. 2021. Understanding long-term groundwater flow at Pahute Mesa and vicinity, Nevada National Security Site, USA, from naturally occurring geochemical and isotopic tracers. *Hydrogeology Journal* **29** (8): 2725–2749 DOI: 10.1007/s10040-021-02397-x

Landwehr JM, Coplen TB. 2006. Line-conditioned excess: A new method for characterizing stable hydrogen and oxygen isotope ratios in hydrologic systems Available at: http://inis.iaea.org/Search/search.aspx?orig_q=RN:37043527 [Accessed 17 May 2019]

Lee SY. 2008. Mangrove macrobenthos: Assemblages, services, and linkages. *Journal of Sea Research* **59** (1): 16–29 DOI: 10.1016/j.seares.2007.05.002

Malzone CM. 1999. Tidal scour and its relation to erosion and sediment transport in Elkhorn Slough.Master Thesis, San Jose State University, San Jose, California, United States.

McKenzie T, Dulai H, Fuleky P. 2021. Traditional and novel time-series approaches reveal submarine groundwater discharge dynamics under baseline and extreme event conditions. *Scientific Reports* **11** (1): 22570 DOI: 10.1038/s41598-021-01920-0

Michael HA, Lubetsky JS, Harvey CF. 2003. Characterizing submarine groundwater discharge: A seepage meter study in Waquoit Bay, Massachusetts. *Geophysical Research Letters* **30** (6) DOI: 10.1029/2002GL016000

Michael HA, Mulligan AE, Harvey CF. 2005. Seasonal oscillations in water exchange between aquifers and the coastal ocean. *Nature* **436** (7054): 1145–1148 DOI: 10.1038/nature03935

Michael HA, Russoniello CJ, Byron LA. 2013. Global assessment of vulnerability to sea-level rise in topography-limited and recharge-limited coastal groundwater systems. *Water Resources Research* **49** (4): 2228–2240 DOI: 10.1002/wrcr.20213

Miklesh D, Meile C. 2018. Porewater salinity in a southeastern United States salt marsh: controls and interannual variation. *PeerJ* **6**: e5911 DOI: 10.7717/peerj.5911

Moffett KB, Gorelick SM, McLaren RG, Sudicky EA. 2012. Salt marsh ecohydrological zonation due to heterogeneous vegetation–groundwater–surface water interactions. *Water Resources Research* **48** (2) DOI: 10.1029/2011WR010874

NERR. 2022. NOAA National Estuarine Research Reserve System (NERRS). System-wide Monitoring Program. Data accessed from the NOAA NERRS Centralized Data Management Office website: www.nerrsdata.org

Neumann B, Vafeidis AT, Zimmermann J, Nicholls RJ. 2015. Future Coastal Population Growth and Exposure to Sea-Level Rise and Coastal Flooding - A Global Assessment. *PLOS ONE* **10** (3): e0118571 DOI: 10.1371/journal.pone.0118571

Nuttle WK, Harvey JW. 1995. Fluxes of water and solute in a coastal wetland sediment. l. The contribution of regional groundwater discharge. *Journal of Hydrology* **164** (1): 89–107 DOI: 10.1016/0022-1694(94)02561-O

Nuttle WK, Hemand HF. 1988. Salt marsh hydrology: Implications for biogeochemical fluxes to the atmosphere and estuaries. *Global Biogeochemical Cycles* **2** (2): 91–114 DOI: 10.1029/GB002i002p00091

Peterson RN, Moore WS, Chappel SL, Viso RF, Libes SM, Peterson LE. 2016. A new perspective on coastal hypoxia: The role of saline groundwater. *Marine Chemistry* **179**: 1–11 DOI: 10.1016/j.marchem.2015.12.005

Povinec PP, Aggarwal PK, Aureli A, Burnett WC, Kontar EA, Kulkarni KM, Moore WS, Rajar R, Taniguchi M, Comanducci J-F, et al. 2006. Characterisation of submarine groundwater discharge offshore south-eastern Sicily. *Journal of Environmental Radioactivity* **89** (1): 81–101 DOI: 10.1016/j.jenvrad.2006.03.008

Povinec PP, Bokuniewicz H, Burnett WC, Cable J, Charette M, Comanducci J-F, Kontar EA, Moore WS, Oberdorfer JA, de Oliveira J, et al. 2008. Isotope tracing of submarine groundwater discharge offshore Ubatuba, Brazil: results of the IAEA–UNESCO SGD project. *Journal of Environmental Radioactivity* **99** (10): 1596–1610 DOI: 10.1016/j.jenvrad.2008.06.010

Price RM, Top Z, Happell JD, Swart PK. 2003. Use of tritium and helium to define groundwater flow conditions in Everglades National Park. *Water Resources Research* **39** (9) DOI: 10.1029/2002WR001929

Putman AL, Fiorella RP, Bowen GJ, Cai Z. 2019. A Global Perspective on Local Meteoric Water Lines: Meta-analytic Insight Into Fundamental Controls and Practical Constraints. *Water Resources Research* **55** (8): 6896–6910 DOI: 10.1029/2019WR025181

R Core Team. 2021. R: A language and environment for statistical computing. R Foundation for Statistical Computing Available at: https://www.R-project.org/

Reeves HW, Thibodeau PM, Underwood RG, Gardner LR. 2000. Incorporation of Total Stress Changes into the Ground Water Model SUTRA. *Groundwater* **38** (1): 89–98 DOI: 10.1111/j.1745-6584.2000.tb00205.x

Robinson CE, Xin P, Santos IR, Charette MA, Li L, Barry DA. 2018. Groundwater dynamics in subterranean estuaries of coastal unconfined aquifers: Controls on submarine groundwater discharge and chemical inputs to the ocean. *Advances in Water Resources* **115**: 315–331 DOI: 10.1016/j.advwatres.2017.10.041

Rocha C, Veiga-Pires C, Scholten J, Knoeller K, Gröcke DR, Carvalho L, Anibal J, Wilson J. 2016. Assessing land–ocean connectivity via submarine groundwater discharge (SGD) in the Ria Formosa Lagoon (Portugal): combining radon measurements and stable isotope hydrology. *Hydrology and Earth System Sciences* **20** (8): 3077–3098 DOI: 10.5194/hess-20-3077-2016

Rosenberry DO, Duque C, Lee DR. 2020. History and evolution of seepage meters for quantifying flow between groundwater and surface water: Part 1 – Freshwater settings. *Earth-Science Reviews* **204**: 103167 DOI: 10.1016/j.earscirev.2020.103167

Rosner B, Grove D. 1999. Use of the Mann–Whitney U-test for clustered data. *Statistics in Medicine* **18** (11): 1387–1400 DOI: 10.1002/(SICI)1097-0258(19990615)18:11<1387::AID-SIM126>3.0.CO;2-V

Rozanski K, Araguás-Araguás L, Gonfiantini R. 1993. Isotopic Patterns in Modern Global Precipitation. In *Climate Change in Continental Isotopic Records*American Geophysical Union (AGU); 1–36. DOI: 10.1029/GM078p0001

Santos IR, Chen X, Lecher AL, Sawyer AH, Moosdorf N, Rodellas V, Tamborski J, Cho H-M, Dimova N, Sugimoto R, et al. 2021. Submarine groundwater discharge impacts on coastal nutrient biogeochemistry. *Nature Reviews Earth & Environment*: 1–17 DOI: 10.1038/s43017-021-00152-0

Schmidt A, Santos IR, Burnett WC, Niencheski F, Knöller K. 2011. Groundwater sources in a permeable coastal barrier: Evidence from stable isotopes. *Journal of Hydrology* **406** (1–2): 66–72 DOI: 10.1016/j.jhydrol.2011.06.001

Schultz BB. 1985. Levene's Test for Relative Variation. *Systematic Biology* **34** (4): 449–456 DOI: 10.1093/sysbio/34.4.449

Shapiro SS, Wilk MB. 1965. An Analysis of Variance Test for Normality (Complete Samples). *Biometrika* **52** (3/4): 591–611 DOI: 10.2307/2333709

Shen C, Jin G, Xin P, Kong J, Li L. 2015. Effects of salinity variations on pore water flow in salt marshes. *Water Resources Research* **51** (6): 4301–4319 DOI: 10.1002/2015WR016911

Sinha E, Michalak AM, Balaji V. 2017. Eutrophication will increase during the 21st century as a result of precipitation changes. *Science* **357** (6349): 405–408 DOI: 10.1126/science.aan2409

Smith CG, Cable JE, Martin JB, Roy M. 2008. Evaluating the source and seasonality of submarine groundwater discharge using a radon-222 pore water transport model. *Earth and Planetary Science Letters* **273** (3–4): 312–322 DOI: 10.1016/j.epsl.2008.06.043

Surano KA, Hudson GB, Failor RA, Sims JM, Holland RC, MacLean SC, Garrison JC. 1992. Heliuim-3 mass spectrometry for low-level tritium analysis of environmental samples. *Journal of Radioanalytical and Nuclear Chemistry Articles* **161** (2): 443–453 DOI: 10.1007/BF02040491

Tamborski JJ, Cochran JK, Bokuniewicz HJ. 2017. Application of 224Ra and 222Rn for evaluating seawater residence times in a tidal subterranean estuary. *Marine Chemistry* **189**: 32–45 DOI: 10.1016/j.marchem.2016.12.006

Tamborski JJ, Eagle M, Kurylyk BL, Kroeger KD, Wang ZA, Henderson P, Charette MA. 2021. Pore water exchange-driven inorganic carbon export from intertidal salt marshes. *Limnology and Oceanography*: lno.11721 DOI: 10.1002/lno.11721

Tamborski JJ, Rogers AD, Bokuniewicz HJ, Cochran JK, Young CR. 2015. Identification and quantification of diffuse fresh submarine groundwater discharge via airborne thermal infrared remote sensing. *Remote Sensing of Environment* **171**: 202–217 DOI: 10.1016/j.rse.2015.10.010

Van Dop M, Hall A, Calhoun K, Kislik C. 2019. Linking land cover and water quality in Elkhorn Slough. Elkhorn Slough Technical Report Series. Elkhorn Slough, CA. Available at: http://library.elkhornslough.org/attachments/VanDop_2019_Linking_Land_Cover_And.pdf [Accessed 11 April 2022]

Van Dyke E, Wasson K. 2005. Historical ecology of a central California estuary: 150 years of habitat change. *Estuaries* **28** (2): 173–189 DOI: 10.1007/BF02732853

Visser A, Broers HP, Bierkens MFP. 2007. Dating degassed groundwater with 3H/3He. *Water Resources Research* **43** (10) DOI: https://doi.org/10.1029/2006WR005847

Visser A, Broers HP, Heerdink R, Bierkens MFP. 2009. Trends in pollutant concentrations in relation to time of recharge and reactive transport at the groundwater body scale. *Journal of Hydrology* **369** (3): 427–439 DOI: 10.1016/j.jhydrol.2009.02.008

Visser A, Broers HP, Purtschert R, Sültenfuß J, de Jonge M. 2013. Groundwater age distributions at a public drinking water supply well field derived from multiple age tracers (^{85}Kr, ^{3}H/ ^{3}He, and ^{39}Ar): Groundwater Age Distributions at a Drinking Water Well Field. *Water Resources Research* **49** (11): 7778–7796 DOI: 10.1002/2013WR014012

Visser A, Thaw M, Deinhart A, Bibby R, Safeeq M, Conklin M, Esser B, Van der Velde Y. 2019. Cosmogenic Isotopes Unravel the Hydrochronology and Water Storage Dynamics of the Southern Sierra Critical Zone. *Water Resources Research* **55** (2): 1429–1450 DOI: 10.1029/2018WR023665

Visser A, Thaw M, Esser B. 2018. Analysis of air mass trajectories to explain observed variability of tritium in precipitation at the Southern Sierra Critical Zone Observatory, California, USA. *Journal of Environmental Radioactivity* **181**: 42–51 DOI: 10.1016/j.jenvrad.2017.10.008

Wang Q, Wang X, Xiao K, Zhang Y, Luo M, Zheng C, Li H. 2021a. Submarine groundwater discharge and associated nutrient fluxes in the Greater Bay Area, China revealed by radium and stable isotopes. *Geoscience Frontiers* **12** (5): 101223 DOI: 10.1016/j.gsf.2021.101223

Wang Q, Xie T, Luo M, Bai J, Chen C, Ning Z, Cui B. 2021b. How hydrological connectivity regulates the plant recovery process in salt marshes. *Journal of Applied Ecology* **58** (6): 1314–1324 DOI: 10.1111/1365-2664.13879

Wang X, Chen X, Liu J, Zhang F, Li L, Du J. 2021c. Radon traced seasonal variations of water mixing and accompanying nutrient and carbon transport in the Yellow-Bohai Sea. *Science of The Total Environment* **784**: 147161 DOI: 10.1016/j.scitotenv.2021.147161

Wilson AM, Gardner LR. 2006. Tidally driven groundwater flow and solute exchange in a marsh: Numerical simulations. *Water Resources Research* **42** (1) DOI: 10.1029/2005WR004302

Wilson AM, Evans TB, Moore WS, Schutte CA, Joye SB. 2015a. What time scales are important for monitoring tidally influenced submarine groundwater discharge? Insights from a salt marsh. *Water Resources Research* **51** (6): 4198–4207 DOI: 10.1002/2014WR015984
Wilson AM, Evans T, Moore W, Schutte CA, Joye SB, Hughes AH, Anderson JL. 2015b. Groundwater controls ecological zonation of salt marsh macrophytes. *Ecology* **96** (3): 840–849 DOI: 10.1890/13-2183.1
Wilson RM, Griffiths NA, Visser A, McFarlane KJ, Sebestyen SD, Oleheiser KC, Bosman S, Hopple AM, Tfaily MM, Kolka RK, et al. 2021. Radiocarbon Analyses Quantify Peat Carbon Losses With Increasing Temperature in a Whole Ecosystem Warming Experiment. *Journal of Geophysical Research: Biogeosciences* **126** (11): e2021JG006511 DOI: 10.1029/2021JG006511
Xiao K, Wilson AM, Li H, Ryan C. 2019. Crab burrows as preferential flow conduits for groundwater flow and transport in salt marshes: A modeling study. *Advances in Water Resources* **132**: 103408 DOI: 10.1016/j.advwatres.2019.103408
Xin P, Kong J, Li L, Barry DA. 2013. Modelling of groundwater–vegetation interactions in a tidal marsh. *Advances in Water Resources* **57**: 52–68 DOI: 10.1016/j.advwatres.2013.04.005
Xin P, Wilson A, Shen C, Ge Z, Moffett KB, Santos IR, Chen X, Xu X, Yau YYY, Moore W, et al. 2022. Surface Water and Groundwater Interactions in Salt Marshes and Their Impact on Plant Ecology and Coastal Biogeochemistry. *Reviews of Geophysics* **60** (1): 1–54 DOI: 10.1029/2021RG000740
Xin P, Yuan L-R, Li L, Barry DA. 2011. Tidally driven multiscale pore water flow in a creek-marsh system. *Water Resources Research* **47** (7) DOI: 10.1029/2010WR010110
Zhang S, Wen X, Wang J, Yu G, Sun X. 2010. The use of stable isotopes to partition evapotranspiration fluxes into evaporation and transpiration. *Acta Ecologica Sinica* **30** (4): 201–209 DOI: 10.1016/j.chnaes.2010.06.003
Zhao L, Wang X, Ma Y, Li S, Wang L. 2021. Investigation and assessment of ecological water resources in the salt marsh area of a salt lake: A case study of West Taijinar Lake in the Qaidam Basin, China. *PLOS ONE* **16** (2): e0245993 DOI: 10.1371/journal.pone.0245993
Zhou Y, Sawyer AH, David CH, Famiglietti JS. 2019. Fresh Submarine Groundwater Discharge to the Near-Global Coast. *Geophysical Research Letters* **46** (11): 5855–5863 DOI: 10.1029/2019GL082749

List of Tables

Table 1. Summary of stable water isotopes of precipitation water collected in Elkhorn Slough. The Date Time start/end refers to the date and time at which the storm event sampled started and ended. We obtained the precipitation amounts from the National Estuarine Research Reserve weather station in Elkhorn Slough (~4.5km from the study site).

Date Time start	Date Time end	δ¹⁸O [‰]	δ¹⁸O SD [‰]	δ²H [‰]	δ²H SD [‰]	Precip amount [mm]
10/21/21 00:00	10/22/21 08:00	-3.08	0.09	-12.02	0.19	0.2
10/25/21 08:00	10/26/21 13:00	-5.86	0.11	-33.74	0.20	0.3
11/23/21 00:00	12/28/21 20:00	-6.14	0.12	-30.2	0.23	63.3
12/28/21 20:00	04/12/22 00:00	-4.87	0.05	-27.73	0.03	208.6

Table 2. Summary of electrical conductivity for precipitation, estuarine (SW), tidal creek, deep groundwater, lower marsh (Low), middle marsh (Mid), upper marsh (Upp), upland (Upl), and hillslope positions (Hill).

	EC [mS/cm]				Wet Season EC [mS/cm]			Dry Season EC [mS/cm]		
Sample	**Min**	**Max**	**Mean**	**n**	**Min**	**Max**	**Mean**	**Min**	**Max**	**Mean**
Precip	0.01	0.2	0.06	4	0.02	0.2	0.11	0.01	0.02	0.02
SW	46.59	60.7	55.3	4	58.3	60.7	59.5	46.6	52.3	49.4
Tidal Creek			24	1			24			
Deep GW	0.8	0.8	0.8	2			0.8	0.8	0.8	0.8
Low	27.7	67.4	58.3	21	27.7	66.7	51.9	53.1	67.4	59.1
Mid	42.9	69.4	61.8	17	42.9	69.5	56.6	56.1	67.0	64.1
Upp	10.4	75.2	54.2	19	10.4	75.3	47.6	51.9	65.7	61.5
Upl	0.02	23.7	5.7	14	2.5	10.2	5.5	0.02	23.7	6.3
Hill	1.7	2.7	2	4	1.7	1.8	1.7	1.9	2.7	2.3

*Table 3. Summary of stable water isotopes and lc-excess for precipitation, estuarine (SW), tidal creek, deep groundwater, lower marsh (Low), middle marsh (Mid), upper marsh (Upp), upland (Upl), and hillslope positions (Hill). * δ^2H volume weighted mean = -28.3 ‰, # $\delta^{18}O$ volume weighted mean = -5.2 ‰.*

	δ¹⁸O [‰]			δ²H [‰]			LC_excess [‰]			
Sample	**Min**	**Max**	**Mean**	**Min**	**Max**	**Mean**	**Min**	**Max**	**Mean**	**n**
Precip	-6.14	-3.08	-4.99#	-33.74	-12.02	-25.92*	5.5	6.5	8.1	4
SW	0.04	0.96	0.37	-1.27	5.34	0.32	-3.08	-1.10	-2.24	4

Tidal Creek			-4.94			-26.01			7.69	1
Deep GW	-5.93	-5.93	-5.93	-37.75	-37.75	-37.75	3.02	3.02	3.02	2
Low	-3.88	1.14	0.03	-19.77	5.69	-0.03	-0.94	-4.02	6.44	21
Mid	-1.91	0.39	-0.24	-12.61	1.76	-2.20	-1.95	-3.57	0.85	17
Upp	-4.47	-0.01	-1.54	-27.94	-1.61	-10.74	-1.12	-3.97	3.30	19
Upl	-5.61	-4.04	-5.14	-34.23	-24.64	-32.22	3.80	0.18	5.96	14
Hill	-5.72	-4.51	-5.25	-37.40	-27.75	-32.38	3.06	1.87	6.09	4

Table 4. Summary statistics of Kruskal-Wallis test showing the effect of wet/dry seasonality in the fractional mix of estuarine surface water for the three salt marsh positions. All the relationships had one degree of freedom and a p-value < 0.01.

Marsh Position	Median fraction wet season estuarine surface water [%]	Median fraction dry season estuarine surface water [%]	Kruskal-Wallis: H
Lower	0.89	1.0	7.8
Middle	0.9	0.98	6.3
Upper	0.64	0.83	8.4

*Table 5. Summary of tritium results in precipitation. *Grande et al. (2022), [#]Harms et al. (2016), [&]unpublished. The error of the weighted mean is the standard error of the mean.*

Date	^{3}H [pCi/L]	^{3}H error [pCi/L]	Precip [mm]	% of WY Precip	Location
03/05/13	6.0	0.4	20	5%	Oakland[#]
02/07/14	6.9	0.6	16	4%	Oakland[#]
03/26/14	4.0	0.4	25	6%	Oakland[#]
03/29/14	14.8	0.8	24	6%	Oakland[#]
02/06/15	4.4	0.3	35	6%	Oakland[#]
07/09/15	11.7	0.5	3	0%	Oakland[#]
09/16/15	5.7	0.2	4	1%	Oakland[#]
11/02/15	7.3	0.4	12	2%	Oakland[#]
11/09/15	8.8	0.6	10	2%	Oakland[#]
11/24/15	12.2	0.6	6	1%	Oakland[#]

10/14/16	10.0	0.5	33	4%	Oakland*
03/03/18	13.1	0.7	1	0%	Oakland*
04/07/18	10.0	0.5	27	5%	Oakland*
03/05/21	4.9	0.2	6	2%	Oakland[&]
03/06/21	4.9	0.3	2	1%	Oakland[&]
03/09/21	9.1	0.9	9	3%	Oakland[&]
03/10/21	10.0	0.4	12	4%	Oakland[&]
03/11/21	11.2	0.5	2	1%	Oakland[&]
03/14/21	13.3	0.6	10	3%	Oakland[&]
10/22/21	6.1	0.4	22	7%	Elkhorn Slough
12/28/21	5.6	0.2	0	0%	Elkhorn Slough
Mean	**8.6**				
St.Dev.	**3.3**				
N	**21**				
Unc.Mean	**0.7**				

Table 6. Summary of tritium ages, recharge flow velocities and recharge rates of subsurface water across the study transect.

Date	Position	Depth [cm]	Age [years]	Age uncertainty [years]	Recharge flow velocity [cm/yr]	Recharge rate [cm/yr]
11/12/20	Upl	250	5.8	1.7	43	13
11/12/20	Hill	430	12.7	1.8	34	13

List of Figures

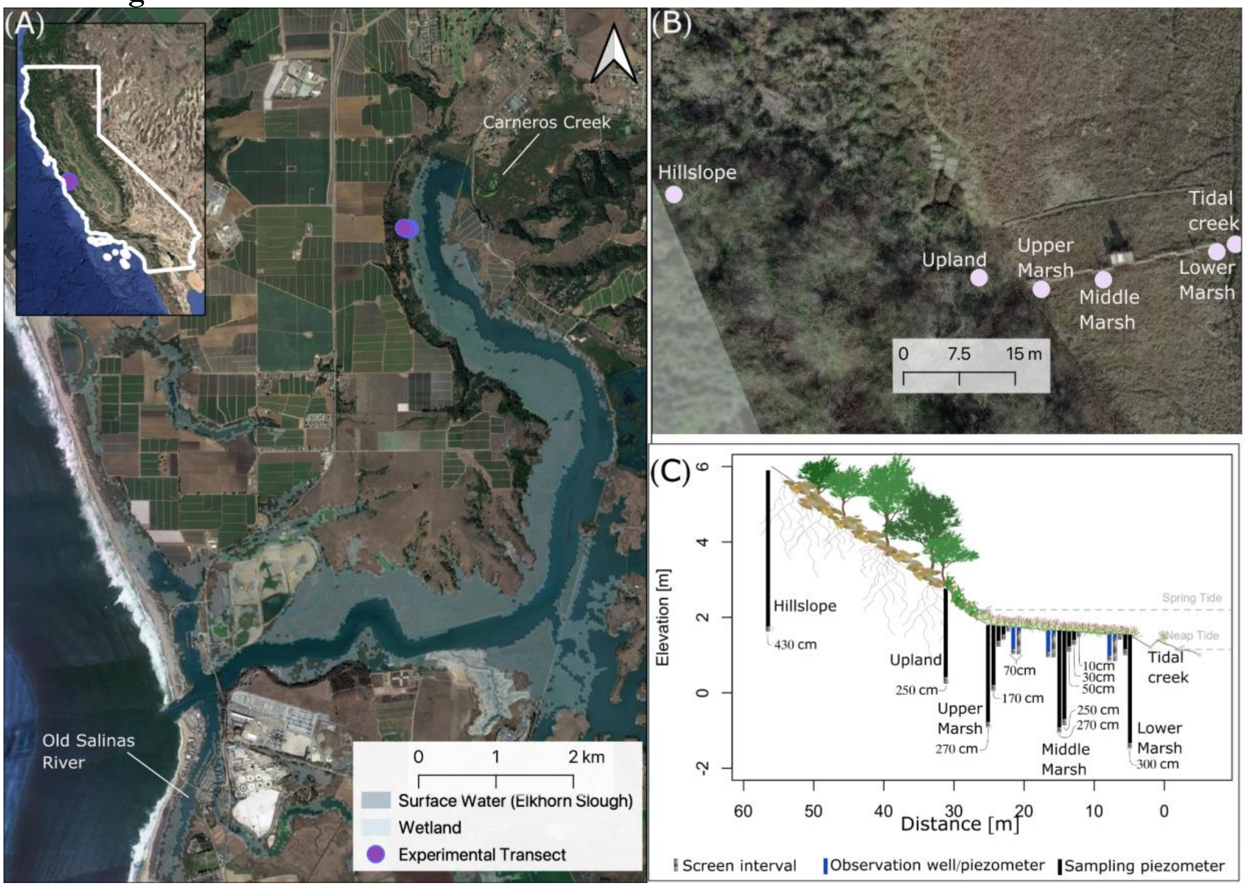

Figure 1. (A) Map of Elkhorn Slough with the extent of wetlands outlined in light blue. The purple symbol marks the location of the study transect. Notice that the experimental transect is adjacent to agricultural fields. (B) Map view of the experimental transect showing the location of the hillslope and upland samling piezometers in relation to the salt marsh transect. (C) Illustration of the experimental transect showing the spatial distribution of the sampling (black) and observation piezometers and wells (blue). The elevation (m relative to NAVD88) of the salt marsh positions are: 1.79 m, 1.65 m, and 1.55 m for the upper, middle, and lower marsh, respectively. The elevation of the hillslope and upland positions is 6 m and 2.4 m, respectively.

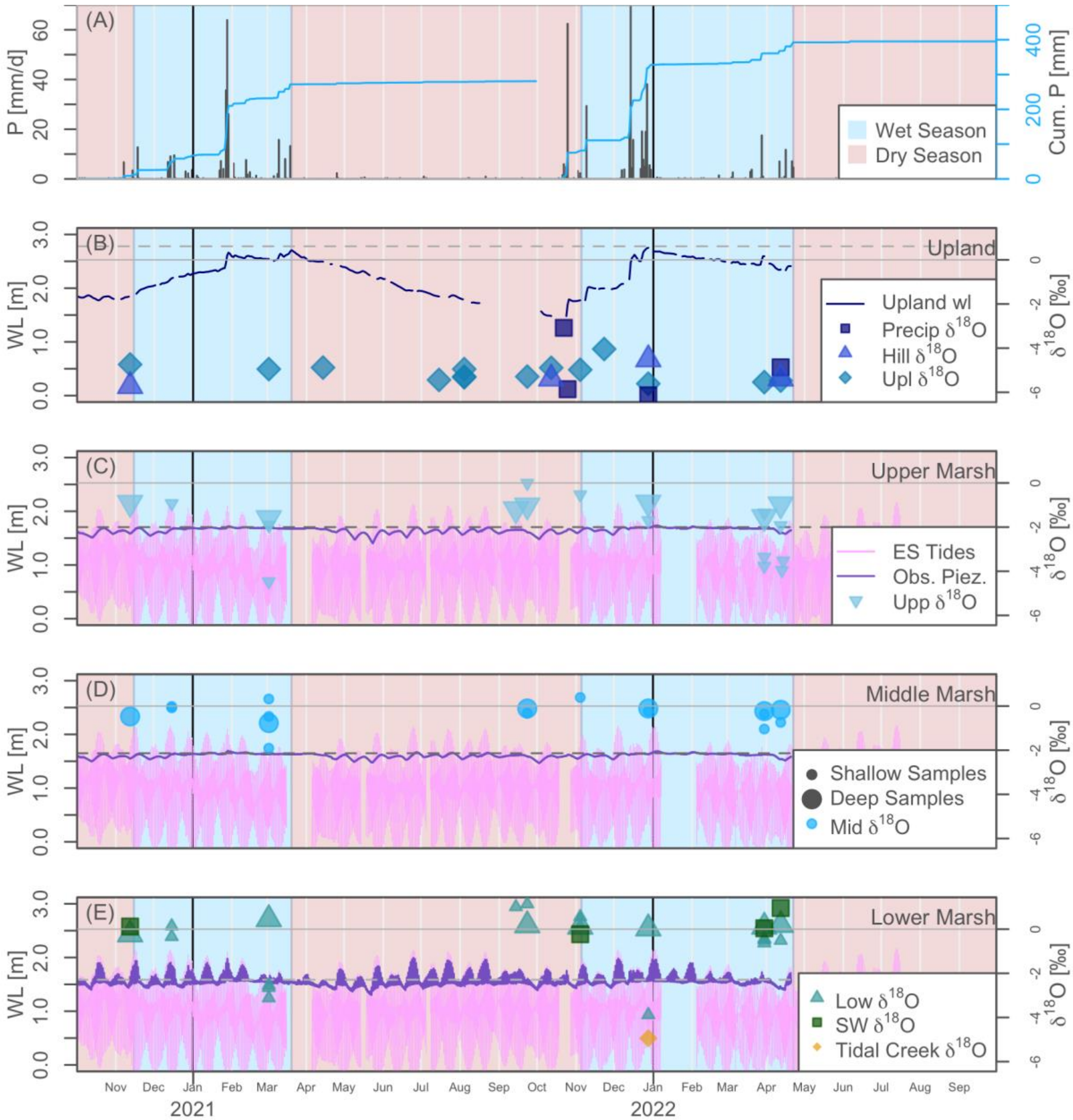

Figure 2. Time series of precipitation (A) and subsurface water level (WL) in the upland (B) and across the salt marsh (C-E). The figure shows data for two water years (2020 and 2021) and illustrates the seasonal variations in the terrestrial water level as measured in the upland position (B). The water level elevations are relative to NAVD88. The Mediterranean climate of the study area, with marked seasonality in precipitation (A), results in a drop of 1.34 m in the terrestrial groundwater level between the rainy and the dry seasons. The horizontal dashed lines in C-E represent the salt marsh elevation at each marsh position. The symbols are $\delta^{18}O$ time series across the different positions. The small symbols correspond to shallow samples (≤ 50 cm-bgs) and the larger symbols correspond to deep samples (> 50 cm-bgs). (C-E) shows the tidal record over the study period(ES Tides). Notice that spring tides flood the salt marsh platform.

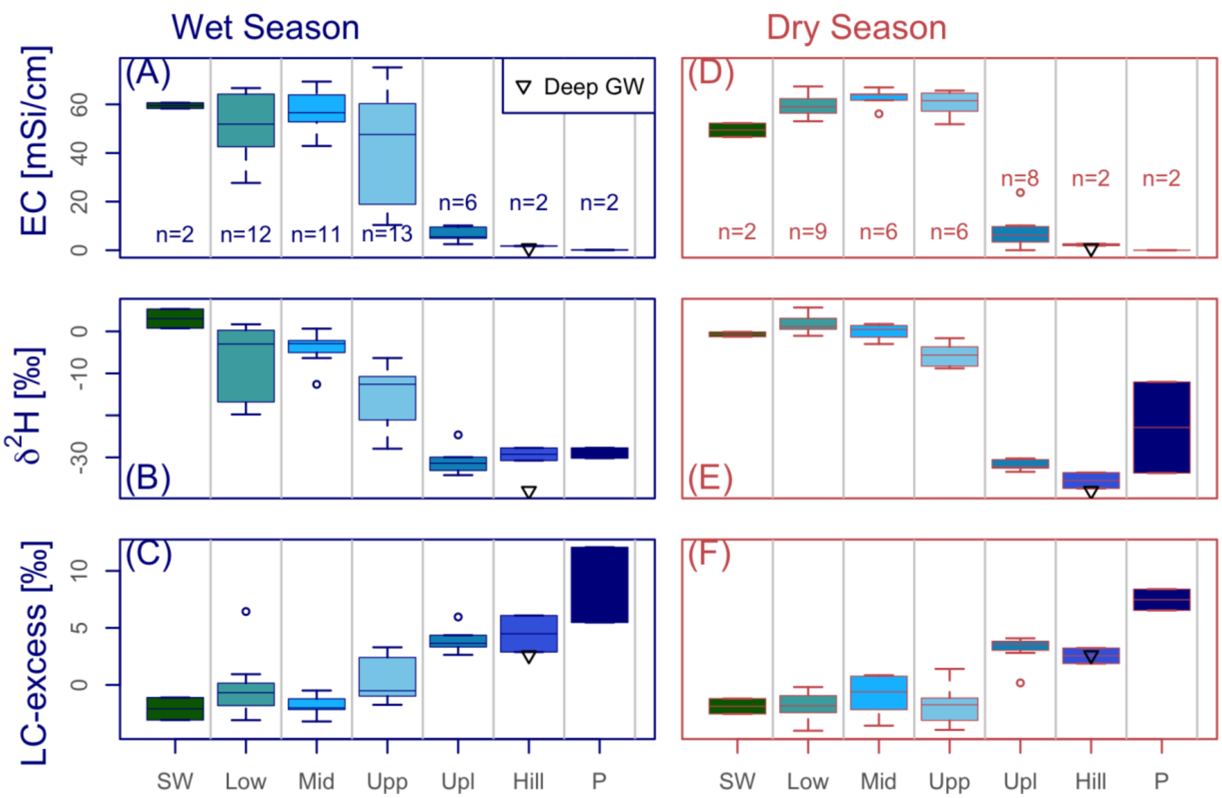

Figure 3. Boxplots of conductivity (A-D), δ^{18}O (B-E) and lc-excess (C-F) for all estuarine/surface water (SW), lower marsh (low), middle marsh (mid), upper marsh (Upp), upland (Upl), and hillslope positions (Hill), and precipitation (P). A-C correspond to the wet season whereas D-F correspond to the dry season. The inverted triangle symbol represents the deep groundwater sample collected from the irrigation well in the agricultural field above the field site (Figure S1).

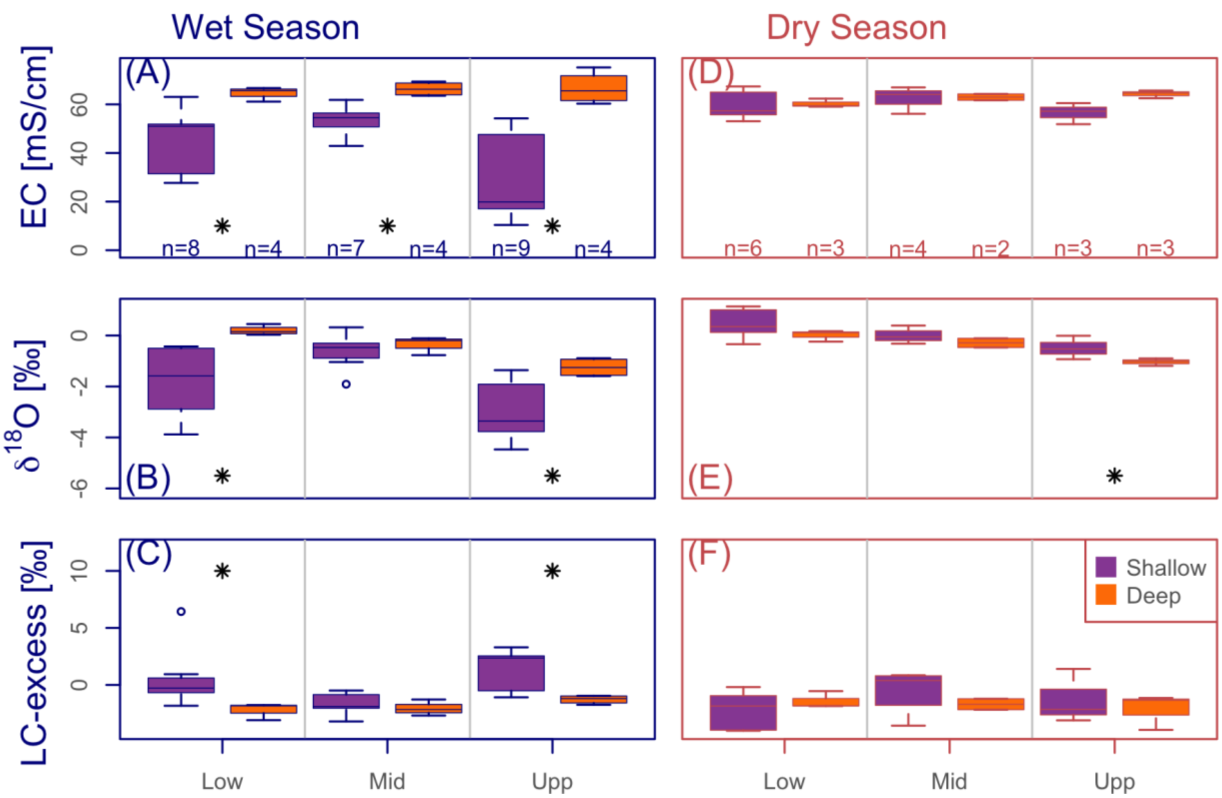

Figure 4. Boxplots of conductivity (A-D), δ^{18}O (B-E) and lc-excess (C-F) for the three marsh positions, lower marsh (low), middle marsh (mid), upper marsh (Upp), separated by shallow (purple) and deep (orange) sampling depths. A-C correspond to the wet season whereas D-F correspond to the dry season. The asterisks demarcate significant differences.

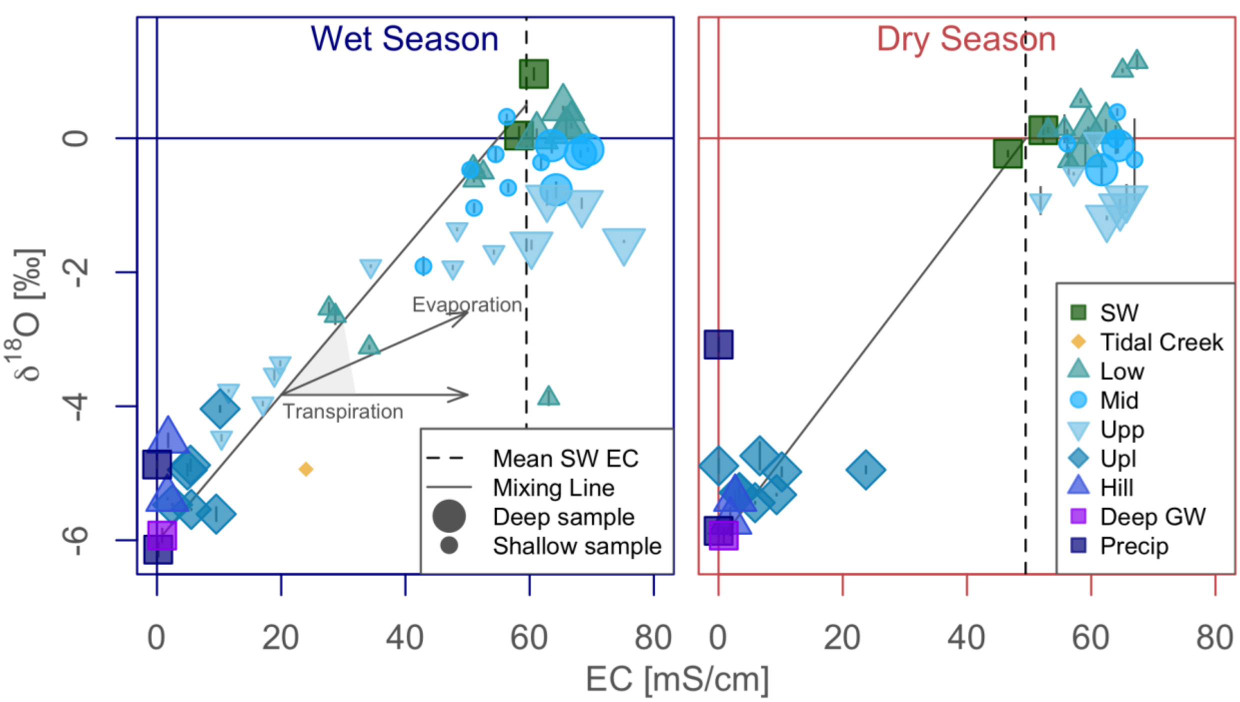

Figure 5. Biplot of $\delta^{18}O$ and electrical conductivity of wet and dry seasons with precipitation (precip), groundwater from the agricultural field adjacent to the study site (Deep GW), Elkhorn Slough surface water (SW), the tidal creek, the lower marsh (Low), the middle marsh (Mid), the upper marsh (Upp), the uland position (Upl), and the hillslope position (Hill). The mixing line connects the deep groundwater, representing the long-term mix of local precipitation, and the mean Elkhorn Slough surface water, representing marine water. All the samples are separated by shape and color (see the figure legend). The size of the points separate shallow (smaller symbols) and deep samples (larger symbols). The error bars are the standard deviation (analytical uncertainty) from individual measurements (notice that in most samples the error bars are within the symbol size).

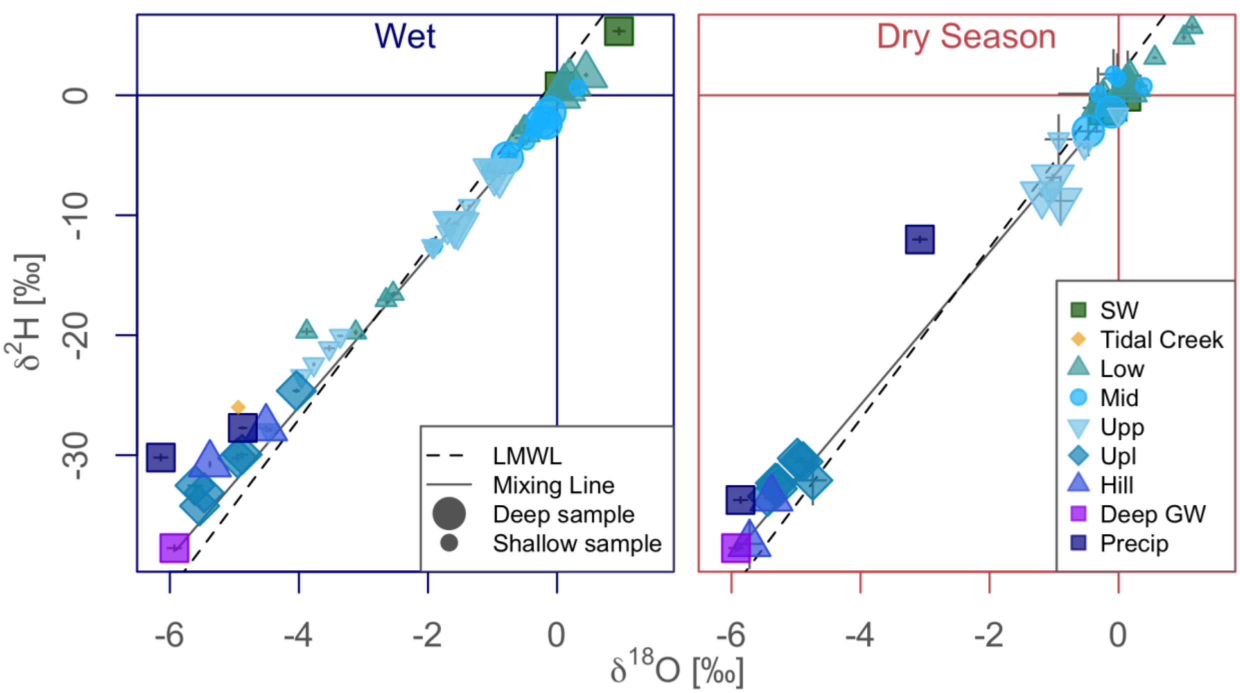

Figure 6. Dual isotope plot of wet and dry seasons with precipitation (precip), groundwater from the agricultural field adjacent to the study site (Deep GW), Elkhorn Slough surface water (SW), the tidal creek, the lower marsh (Low), the middle marsh (Mid), the upper marsh (Upp), the uland position (Upl), and the hillslope position (Hill). The local meteoric water line (LMWL) is : $\delta^2H = 7.1 \times \delta^{18}O + 1.6$. The mixing line connects the deep groundwater, representing the long-term mix of local precipitation, and the mean Elkhorn Slough surface water, representing marine water. All the samples are separated by shape and color (see the figure legend). The size of the points separate shallow (smaller symbols) and deep samples (larger symbols). The error bars are the standard deviation (analytical uncertainty) from individual measurements (notice that in most samples the error bars are within the symbol size).

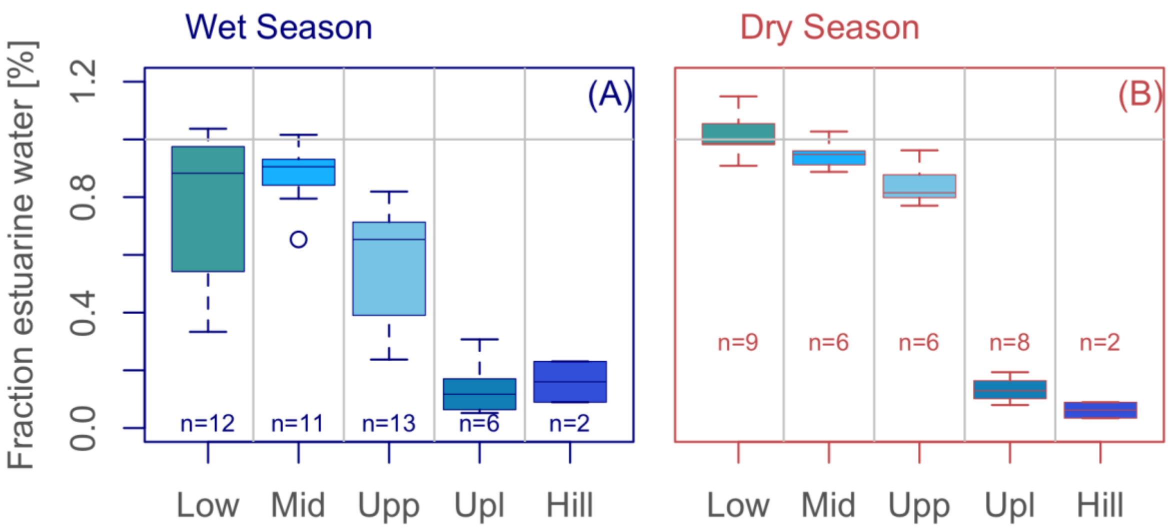

Figure 7. Boxplots of fractions of estuarine water (Elkhorn Slough) across the different positions for the wet (A) and dry seasons (B) calculated using $\delta^{18}O$ as a tracer. Notice that during the dry season, some salt marsh samples are isotopically heavier than Elkhorn Slough water.

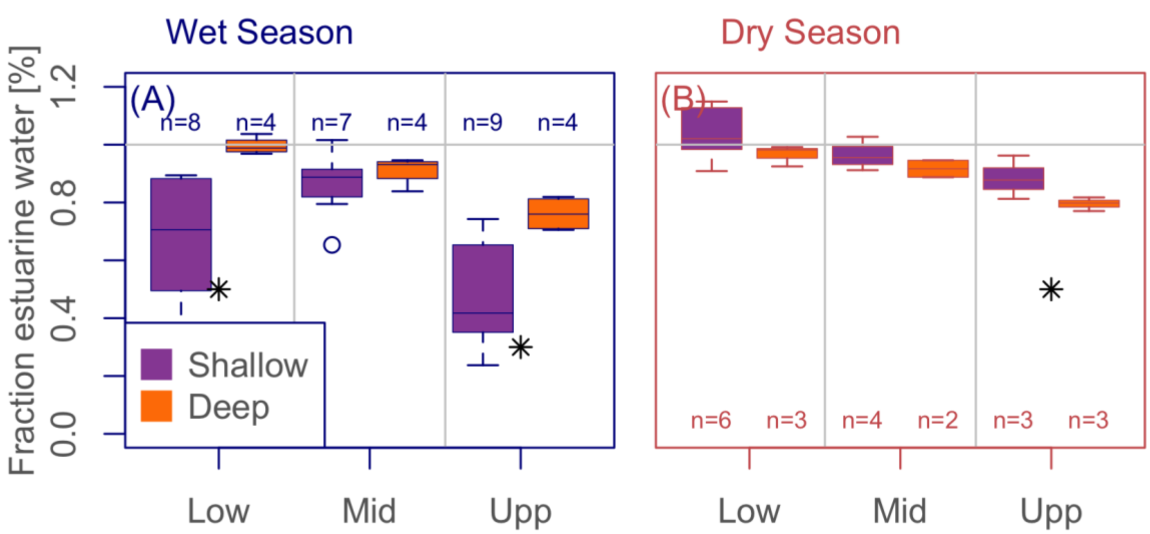

Figure 8. Boxplot of fractional mix of Elkhorn Slough water in the three salt marsh positions separated by wet (A) and dry seasons (B). The asterisks demarcate significant differences.

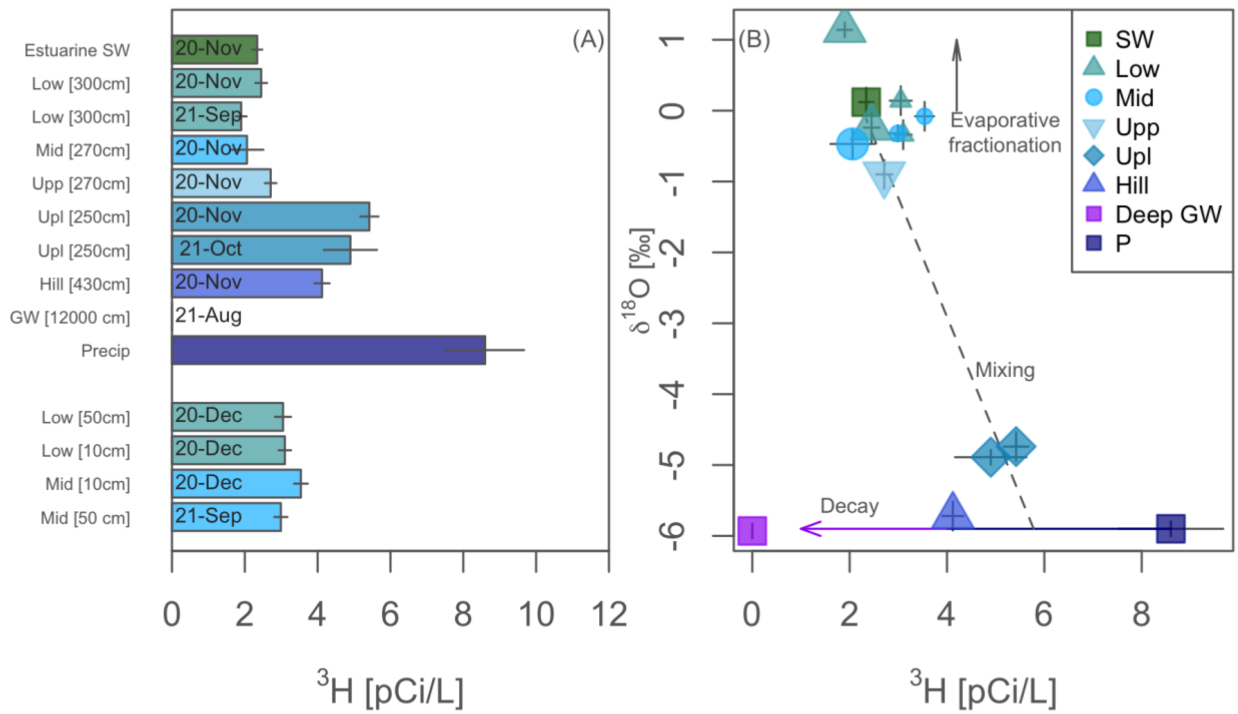

Figure 9. Barplot of tritium in subsurface water (A) and δ^{18}O and ^{3}H biplot illustrating the mixing and decay processes for the different positions (B). The terrestrial age was calculated from the interception of the mixing line and the decay lines. The labels in the bars in (A) are the month/year when the samples were collected. The names of each sample in (A) also shows the depth of the sample in brackets. The error bars are the analytical error. The error bar of the precipitation is the standard error of the mean. GW is the deep groundwater sample.

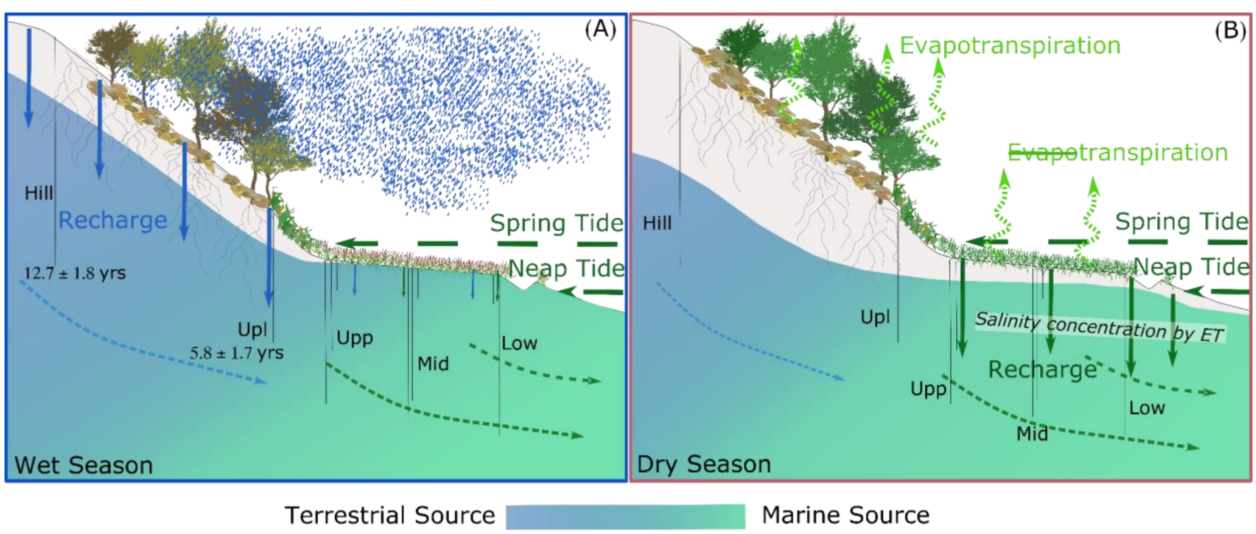

Figure 10. Conceptual model of the study transect for the wet (A) and dry seasons (B). Semidiurnal, the salt marsh is flooded resulting in surface water-subsurface water exchanges. Frequent flushing of shallow subsurface water in the marsh results in subsurface water ages in the order of ~0 yrs, while subsurface water ages at depth increase from the hillslope towards the lower marsh. The dashed arrows in the subsurface indicate the major flow pathways. Vertical arrows represent subsurface recharge to the terrestrial aquifer (blue) and the salt marsh (green). Although subsurface water is super-saline, we did not find any evaporative signal in our samples, indicating that plant transpiration is a first order driver increasing salinity in subsurface water. The salt marsh subsurface is recharged during the dry season.

Supporting information for:

Flow directions and ages of subsurface water in a Mediterranean salt marsh system constrained by isotope tracing

Authors: Emilio Grande[1,2*], Ate Visser[3], Erik Oerter[3], Bhavna Arora[4],Erin C. Seybold[5], Corianne Tatariw[6], Anna Braswell[7,8], Maya Montalvo[1,a], Margaret Zimmer[1]

[1] University of California Santa Cruz, Department of Earth and Planetary Sciences, Santa Cruz, CA, United States
[2] California State University East Bay, Department of Earth and Environmental Sciences, Hayward, CA, United States
[3] Lawrence Livermore National Laboratory, Nuclear and Chemical Sciences Division, Livermore, CA, United States
[4] Lawrence Berkeley National Laboratory, Energy Geosciences Division, Berkeley, CA, United States
[5] University of Kansas, Kansas Geological Survey, Lawrence, KS, United States
[6] University of Alabama, Department of Biological Sciences, Tuscaloosa, AL, United States
[7] University of Florida, School of Forest Resources and Conservation, Fisheries and Aquatic Sciences Program, Gainesville, FL, United States
[8] University Florida Sea Grant, Institute of Food and Agricultural Sciences, Gainesville, FL, United States
[a] Now at Simon Fraser University, Department of Geography, Burnaby, BC, Canada

Corresponding author: Emilio Grande
Department of Earth and Environmental Sciences, California State University East Bay, Hayward, CA 94542. email: emilio.grande@csueastbay.edu

Content of this file

Figures S1 to S4

Text S1

Table S1 to S6

Introduction

Here we provide supplementary figures and tables. Figures provide (1) an elevation model of the study area showing some of the geomorphologic features of the site that provide surface runoff onto the salt marsh (2) time series (hourly time steps) of the meteorological parameters available for this study (3) stable water isotope biplot illustrating the deviation of local precipitation collected in the 2022 water year from the long-term local meteoric water line and (4) a plot of lc-excess versus $\delta^{18}O$ showing minimal evaporative fractionation in the salt marsh subsurface (5) a plot of tritium activity in precipitation versus several hydroclimatic parameters.

The text S1 provides an explanation of the analysis of apparent tritium ages and lumped parameter models to interpret tritium values

The table provides (1) summary of depth and the type (observation versus sampling) piezometers used in the study (2) summary schedule of isotope and conductivity sampling/measurement (3) summary p-value of multiple pairwise Mann-Whitney U test for electrical conductivity across the experimental transect (4) summary p-value of multiple pairwise Mann-Whitney U test for δ^2H across the experimental transect (5) summary p-value of multiple pairwise Mann-Whitney U test for lc-excess across the experimental transect (6) summary p-value of multiple pairwise Mann-Whitney U test for fractional mixing of Elkhorn Slough water across the experimental transect

Figure S1. Map of the study site

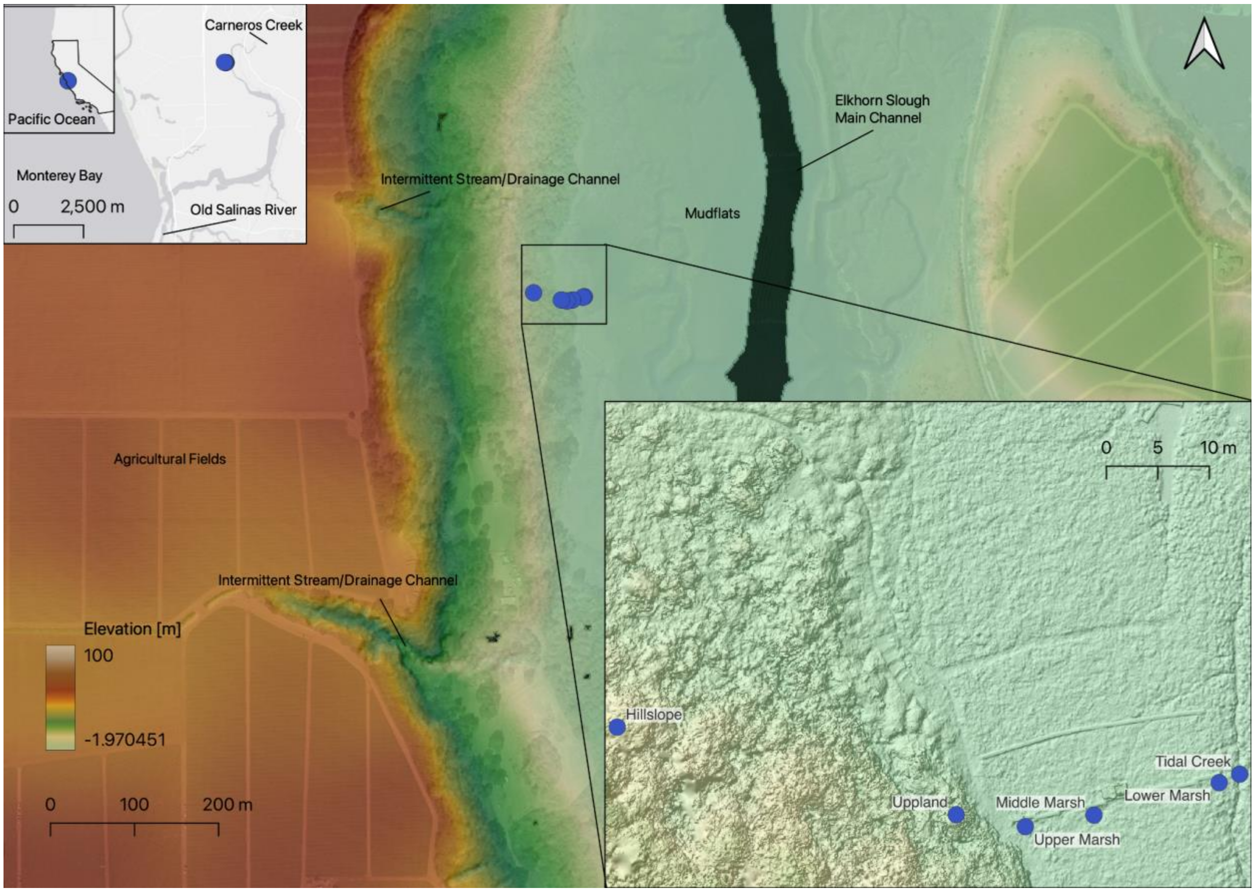

Figure S1. Map of the study site showing the elevation gradient of the area. The figure highlights the geomorphological features that provide pathways for surface runoff onto the salt marsh during precipitation events. The inset shows a high resolution DEM of the experimental transect, illustrating some of the salt marsh features such as the tidal creek.

1118 **Figure S2.** Time series of meteorological data available for the study

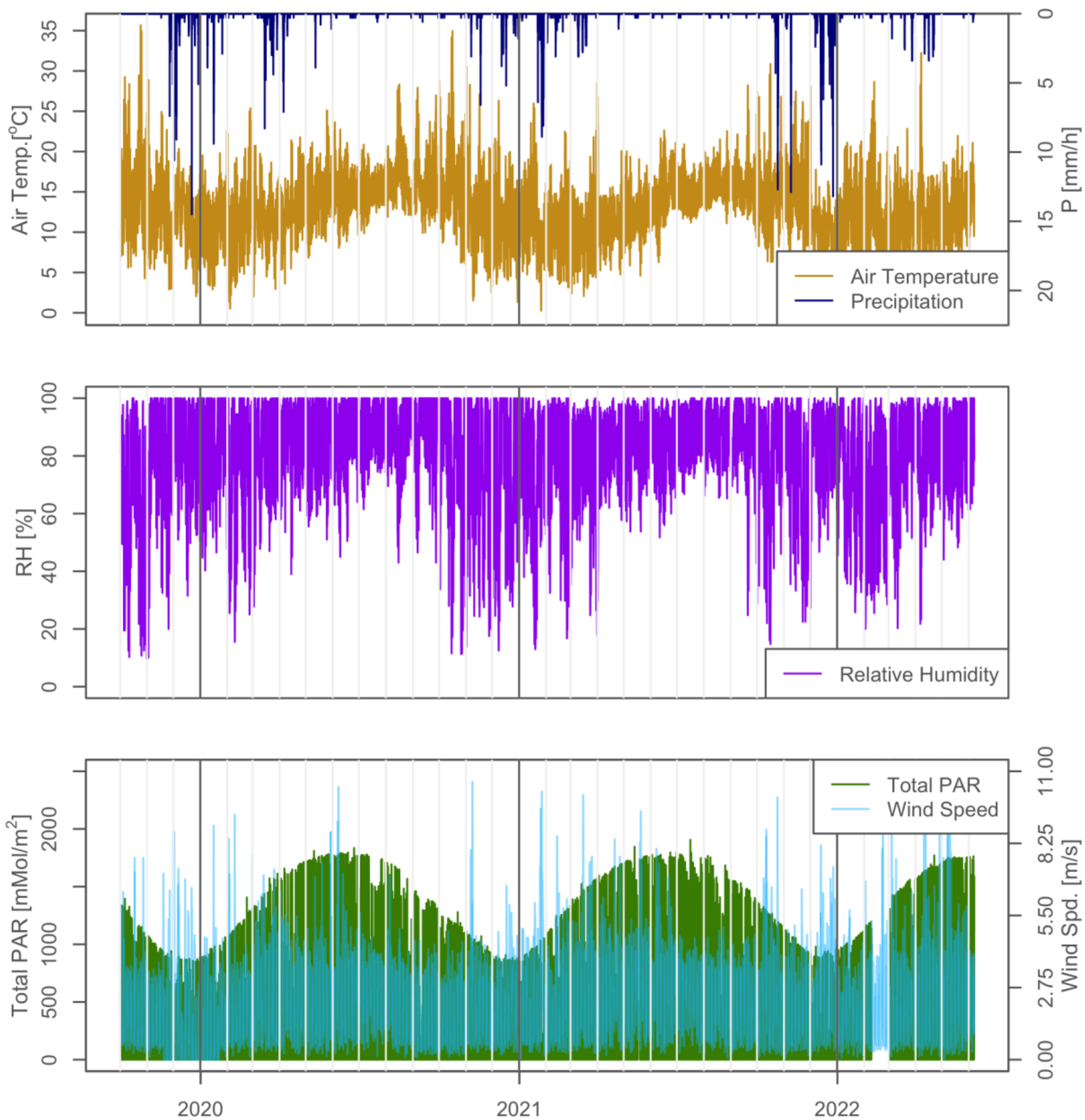

1119

1120 *Figure S2. Time series of all the meteorological variables available for the study (hourly). Meteorological data is*
1121 *measured through the Elkhorn SLough National Estuarine Research Reserve ~4.5 km from the study site. PAR is*
1122 *photosynthetically active radiation.*

Figure S3. Stable water isotopes biplot

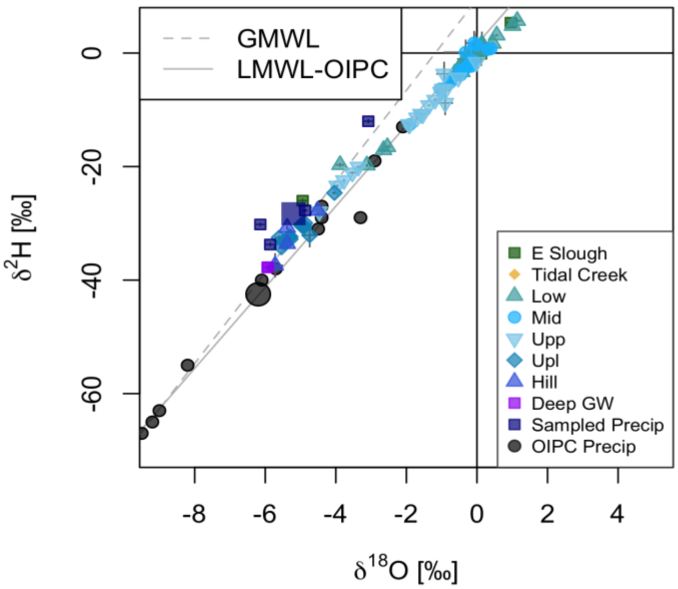

Figure S3. Dual isotope plot illustrating the deviation of the local meteoric water line (LMWL) obtained from the online isotope in precipitation calculator (OIPC). Notice that the precipitation samples, collected at the site during the 2022 water year, deviate from the long-term estimates that form the LMWL. The figure also illustrates the global meteoric water line (GMWL). The volume weighted sampled precipitation and the annual average isotopic compositions per the OIPC at the cite are shown by the larger size symbols.

1131 **Figure S4.** lc-excess versus $\delta^{18}O$

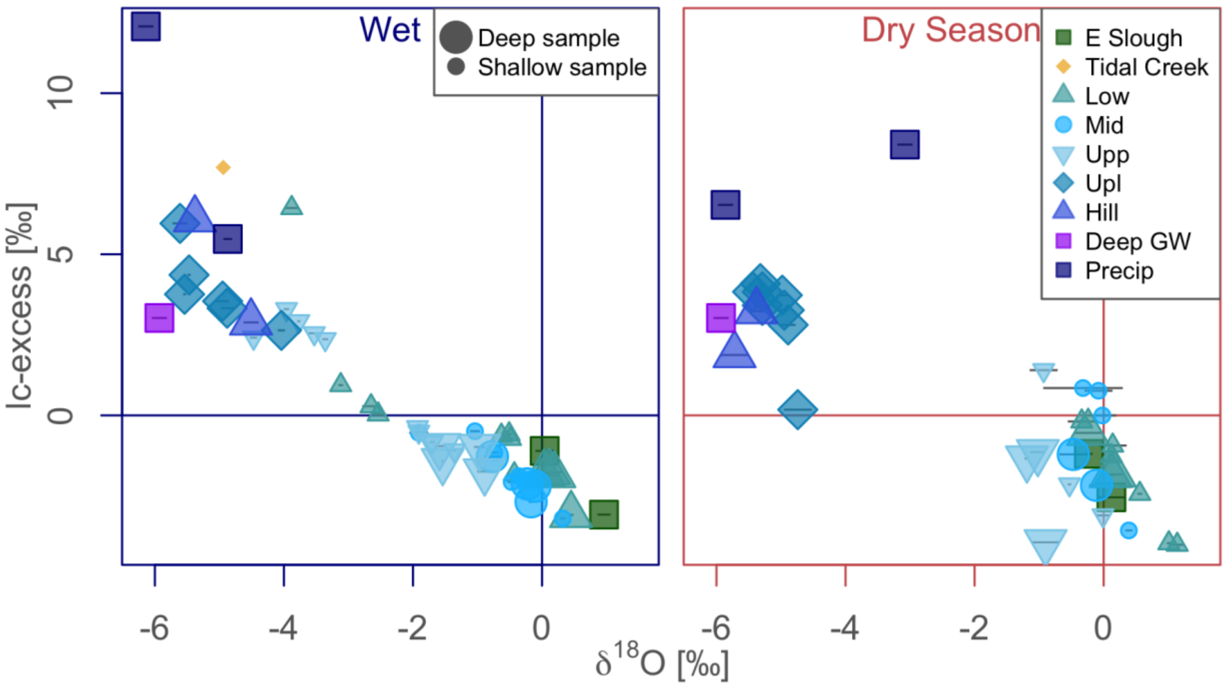

1132

1133 *Figure S4. Line conditioning excess versus $\delta^{18}O$ biplot. The figure shows that there is no significant*
1134 *evaporative fractionation in the salt marsh subsurface.*

1135

Figure S5. Plot of tritium activity in precipitation versus several hydroclimatic parameters

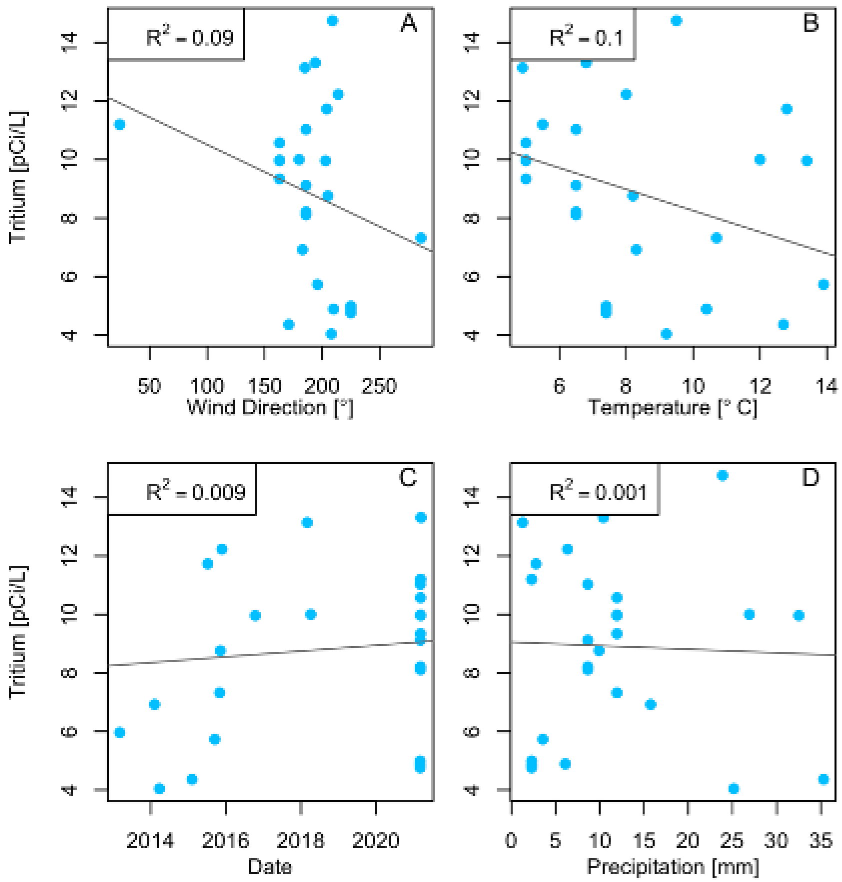

Figure S5. Tritium activity in precipitation v. wind direction (A), air temperature (B), time (C), and precipitation depth (D).

Text S1- Analysis of apparent tritium ages and lumped parameter models to interpret tritium values

To examine the validity and accuracy of the apparent tritium ages, we compared the measured tritium concentrations to the exponential and dispersion mixing models. For the dispersion model, we used a dispersion parameter ranging from 0.005 to 0.5. The tritium input was based on Harms, multiplied by 1.06 to obtain the present-day tritium concentration in precipitation of 8.6 pCi/L.

Figure S1 shows the initial tritium in precipitation, corrected for decay up to 2020 (i.e. piston flow model), as well as tritium concentrations predicted by various dispersion and exponential models. Dispersion models with small dispersion parameters closely follow the tritium in precipitation while larger dispersion parameters smooth the peak of tritium in precipitation that occurred 50-60 yrs ago. The tritium concentration of the exponential model is continuously decreasing with age.

The tritium concentrations measured in the deep terrestrial piezometers (Upland=N4, Hillslope=N5) are plotted at their respective apparent tritium ages (larger symbols) as well as the youngest model age that results in the same tritium value (smaller symbols). For dispersion models with a parameter of 0.1 or smaller, the model ages are close to the apparent ages. For larger dispersion parameters and the exponential model, there is a substantial difference between the model and apparent ages, in particular for the Hillslope (N5) deep piezometer. For both piezometers, additional possible ages on the rising and falling edge of the bomb pulse are possible (but not plotted here). While these older age estimates are hypothetically possible, given the assumptions underlying these lumped parameter models, their hydrological interpretation is less probable. For example, age interpretations around the falling edge of the bomb pulse (~40 yrs old) require very low recharge rates (2-4 mm/yr) typically associated with desert environments.

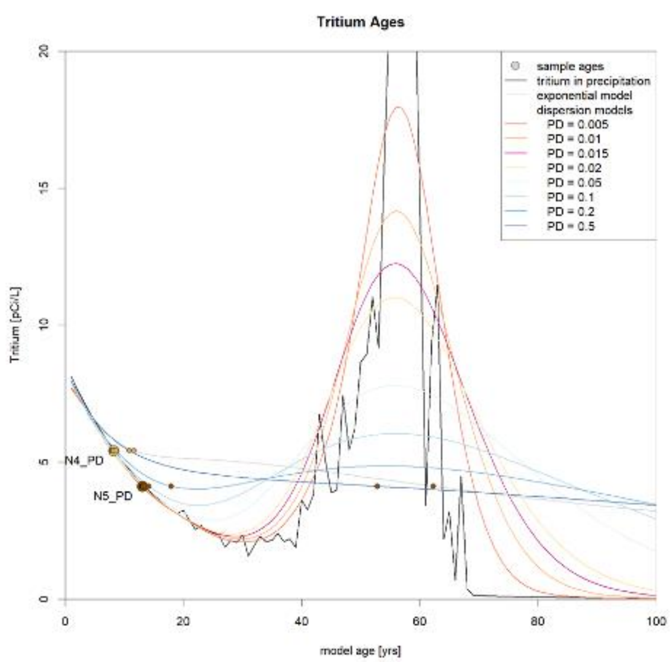

Figure 1 Text S1: Measured tritium concentrations in Upland (N4) and Hillslope (N5) deep piezometers, together with initial tritium in precipitation, corrected for decay up to 2020 (i.e. piston flow model) and tritium concentrations predicted by various dispersion and exponential models.

Figure S2 shows the cumulative age distributions associated with the first intersection of the measured and modeled tritium values (as illustrated in Fig S1). Although the mean age for N4 is larger for the exponential model and the dispersion model with PD=0.5, the median age (where the cumulative age distribution reaches 0.5) for all age models is very similar. For N5, the median age of the exponential and PD=0.5 models are substantially different.

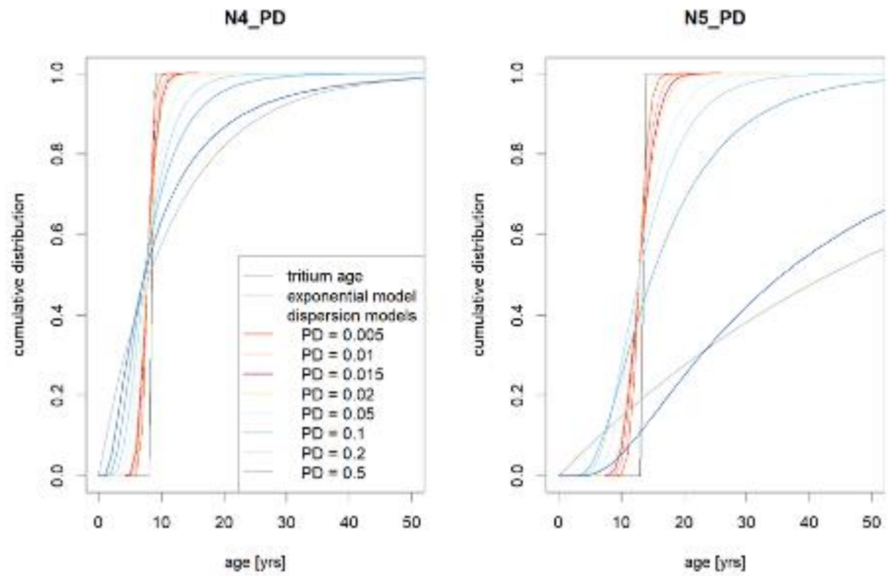

Figure 2 TextS1: Cumulative age distributions associated with the various lumped parameter models for the Upland (N4) and Hillslope (N5) deep piezometers

Repeated tritium measurements over the course of 16 months show stable tritium concentrations in both piezometers, suggesting that dispersion along subsurface flow paths reduce observed seasonal and interannual variability in precipitation (Table 1 Text S1). Constraining the magnitude of dispersion (PD parameter) is hypothetically possible but beyond the scope of this study.

Table 1 Text S1. Tritium activity in the upland and hillslope across wet and dry seasons.

Position	**Depth (cm)**	**Date**	**Tritium (pCi/L)**	**Uncertainty (pCi/L)**
Upland	250	12/16/2020	5.42	0.25
Upland	250	9/23/2021	5.22	0.25
Upland	250	12/28/2021	5.47	1.50
Upland	250	4/12/2022	5.40	0.35
Hillslope	430	12/16/2020	4.12	0.21
Hillslope	430	10/12/2021	4.22	0.35
Hillslope	430	12/28/2021	4.15	0.21
Hillslope	430	4/12/2022	6.06	0.59

Table S1. Summary of depth and the type of well/piezometer used in the study by depth and position

Position	well/piezometer	Depth [cm]	Pressure transducer?	sampling?
Lower Marsh	piezometer	10	no	yes
Lower Marsh	piezometer	50	no	yes
Lower Marsh	well	70	yes	no
Lower Marsh	piezometer	70	yes	no
Lower Marsh	piezometer	300	yes*	yes
Middle Marsh	piezometer	10	no	yes
Middle Marsh	piezometer	30	no	yes
Middle Marsh	piezometer	50	no	yes
Middle Marsh	well	70	yes	no
Middle Marsh	piezometer	70	yes	no
Middle Marsh	piezometer	250	no	yes
Middle Marsh	piezometer	270	no	yes
Upper Marsh	piezometer	10	no	yes
Upper Marsh	piezometer	30	no	yes
Upper Marsh	piezometer	50	no	yes
Upper Marsh	well	70	yes	no
Upper Marsh	piezometer	70	yes	no
Upper Marsh	piezometer	170	yes*	yes
Upper Marsh	piezometer	270	yes*	yes
Uppland	piezometer	250	yes	yes
Hillslope	piezometer	430	no	yes

**Data was not used in this study*

Table S2. Summary schedule of water isotopes and conductivity samples

Sample Type	Position	Depth [cm]	Fall 2020	Winter 2021	Spring 2020	Summer 2021	n
Precipitation	-	-		x	x		4
Elkhorn Slough Surface Water	-	-	x		x		3
Tidal Creek	-	-		x			1
Deep Groundwater	-	4000		x			2
Subsurface Water	Lower Marsh	10	x				1
Subsurface Water	Lower Marsh	50	x	x	x	x	5
Subsurface Water	Lower Marsh	300	x	x	x	x	5
Subsurface Water	Middle Marsh	10	x				1
Subsurface Water	Middle Marsh	30	x				1
Subsurface Water	Middle Marsh	50	x	x	x		4
Subsurface Water	Middle Marsh	250		x	x	x	3
Subsurface Water	Middle Marsh	270	x		x		2
Subsurface Water	Upper marsh	10			x		1
Subsurface Water	Upper marsh	30			x	x	2
Subsurface Water	Upper marsh	50	x		x	x	4
Subsurface Water	Upper marsh	170		x	x	x	3
Subsurface Water	Upper marsh	270	x		x	x	4
Subsurface Water	Upland	250	x	x	x	x	8
Subsurface Water	Hillslope	430	x	x	x	x	4

Table S2. Summary schedule of stable water isotopes and conductivity samples

Table S3. Summary p-value of Kruskal-Wallis test of electrical conductivity amongst all marsh positions

	SW	**Tidal Creek**	**Low**	**Mid**	**Upp**	**Upl**	**Hill**	**GW**
Tidal Creek	0.12	-	0.11	0.11	0.25	0.12	0.16	0.16
Low	0.5	0.11	-	0.3	0.35	**0.0001**	**0.002**	**0.02**
Mid	0.2	0.11	0.3	-	**0.0001**	**0.0001**	**0.002**	**0.02**
Upp	0.9	0.25	0.35	**0.0001**	-	0.09	**0.002**	**0.03**
Upl	**0.003**	0.12	**0.0001**	**0.0001**	0.09	-	**0.01**	0.06
Hill	**0.02**	0.16	**0.002**	**0.002**	**0.002**	**0.01**	-	0.06
GW	**0.06**	0.16	**0.02**	**0.02**	**0.03**	0.06	0.06	-
P	**0.02**	0.15	**0.004**	**0.004**	**0.003**	**0.02**	**0.02**	**0.06**

Table S3. Summary p-value of Kruskal-Wallis test of electrical conductivity amongst all marsh positions. Boded values represent significant differences in the mean rank of EC between the two positions.

Table S4. Summary p-value of Kruskal-Wallis test of δ^2H amongst all marsh positions

	SW	**Tidal Creek**	**Low**	**Mid**	**Upp**	**Upl**	**Hill**	**GW**
Tidal Creek	0.2	-	0.09	0.1	0.14	0.16	0.2	0.22
Low	0.5	**0.09**	-	0.3	**0.0002**	**0.0001**	**0.002**	**0.002**
Mid	0.06	0.1	0.3	-	**0.0001**	**0.0001**	**0.002**	**0.02**
Upp	**0.002**	0.14	**0.0002**	**0.0001**	-	**0.0001**	**0.003**	**0.02**
Upl	**0.003**	0.16	**0.0001**	**0.0001**	**0.0001**	-	0.5	**0.02**
Hill	**0.03**	0.2	**0.002**	**0.002**	**0.003**	0.5	-	0.06
GW	0.08	0.22	**0.002**	**0.02**	**0.02**	**0.02**	0.06	-
P	**0.03**	0.48	**0.004**	**0.003**	**0.01**	0.2	0.9	0.06

Table S4. Summary p-value of Kruskal-Wallis test of δ^2H amongst all marsh positions. Boded values represent significant differences in the mean rank of δ^2H between the two positions.

Table S5. Summary p-value of Kruskal-Wallis test of lc-excess amongst all marsh positions

	ES	Hill	GW	Low	Mid	P	Tidal Creek	Upl
Hill	0.2		0.3	0.6	0.09	**0.003**	**0.03**	0.08
GW	0.3	0.3		0.4	0.2	**0.0001**	**0.005**	**0.04**
Low	0.6	0.6	0.4		0.05	**0.0001**	**0.002**	**0.02**
Mid	0.09	0.09	0.2	0.05		**0.0001**	**0.01**	**0.04**
P	**0.003**	**0.003**	**0.0001**	**0.0001**	**0.0001**		0.5	0.2
Tidal Creek	**0.03**	**0.03**	**0.005**	**0.002**	**0.01**	0.5		**0.04**
Upl	0.08	0.08	**0.04**	**0.02**	**0.04**	0.2	1	
Upp	**0.03**	1	**0.002**	**0.002**	**0.002**	**0.004**	**0.04**	0.06

Table S5. Summary p-value of Kruskal-Wallis test of lc-excess amongst all marsh positions. Boded values represent significant differences in the mean rank of lc-excess between the two positions.

Table S6. Summary p-value of Kruskal-Wallis test of fractional mixing of Elkhorn Slough water amongst all marsh positions

	Low	Mid	Upp	Upl
Mid	0.3	-	**0.001**	**0.0001**
Upp	**0.0001**	**0.001**	-	**0.0001**
Upl	**0.0001**	**0.0001**	**0.0001**	-
Hill	**0.002**	**0.002**	**0.003**	0.5

Table S5. Summary p-value of Kruskal-Wallis test of fractional mixing of Elkhorn Slough water amongst all marsh positions. Boded values represent significant differences in the mean rank of fractional mixing of Elkhorn Slough water between the two positions.